Inorganic Chemistry

Article

pubs.acs.org/IC

$[Mn^{III}(Schiff\ Base)]_3[Re^{IV}(CN)_7]$, Highly Anisotropic 3D Coordination Framework: Synthesis, Crystal Structure, Magnetic Investigations, and Theoretical Analysis

Denis G. Samsonenko,[†,‡] Carley Paulsen,*[,§] Elsa Lhotel,[§] Vladimir S. Mironov,*[,⊥] and Kira E. Vostrikova*[,†,∥]

[†]Nikolaev Institute of Inorganic Chemistry, SB RAS, 3 Lavrentiev Avenue, Novosibirsk 630090, Russia

[‡]Novosibirsk State University, 2 Pirogova Street, Novosibirsk 630090, Russia

[§]Institut Néel, CNRS & Université Joseph Fourier, 25 Rue des Martyrs, 38042 Grenoble, France

[∥]Laboratoire des Multimatériaux et Interfaces, UMR 5615, Université Claude Bernard Lyon 1, Bat. Chevreul, 43 bd du 11 Novembre 1918, 69622 Villeurbanne, France

[⊥]A. V. Shubnikov Institute of Crystallography, RAS, 59 Leninsky Avenue, 119333 Moscow, Russia

Supporting Information

ABSTRACT: A new highly anisotropic coordination heterobimetallic polymer $[Mn^{III}(Schiff\text{-}base)]_3[Re^{IV}(CN)_7]$ was synthesized and characterized structurally and magnetically. The single crystal X-ray analysis has revealed that this is the first framework among the complexes composed of homoleptic cyanometallate and Mn^{III} complex of the tetradentate Schiff base ligand. A formation of 3D assembly is possible due to both the pentagonal bipyrimidal geometry of the cyanometallate unit and suitable size of constituents: $[Re(CN)_7]^{3-}$ and $[Mn^{III}(acacen)]^+$, where acacen = *N*,*N*′-ethylenebis(acetylacetoneiminato). The powder and crystal magnetic studies show that the compound undergoes an antiferromagnetic ordering of a complicated character below Neel temperature of 13 K, and exhibits a metamagnetic behavior and strong magnetic anisotropy similar to those observed in related 3D Mn^{II}−$[Mo(CN)_7]^{4-}$ systems. Unusual magnetic properties of $[Mn^{III}(acacen)]_3[Re^{IV}(CN)_7]$ (**1**) originate from an interplay of Re−Mn anisotropic spin coupling and ZFS effect of Mn^{III} ions with a noncollinear orientation of the local magnetic axes in the cyano-bridged 3D network. A theoretical model of anisotropic spin coupling between orbitally degenerate $[Re^{IV}(CN)_7]^{3-}$ complexes and Mn^{III} ions is developed, and specific microscopic mechanisms of highly anisotropic spin coupling in Re^{IV}−CN−Mn^{III} linkages in complex **1** are analyzed in detail.

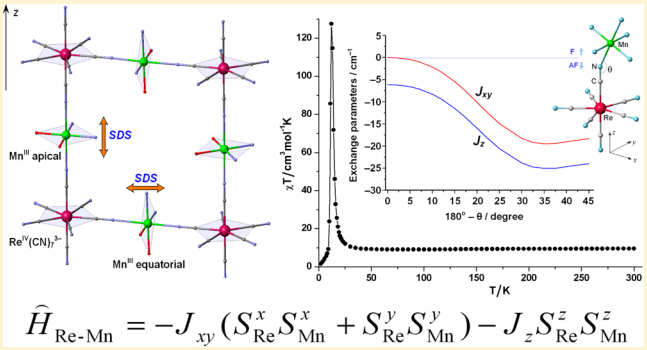

$$\hat{H}_{\text{Re-Mn}} = -J_{xy}(S^x_{\text{Re}}S^x_{\text{Mn}} + S^y_{\text{Re}}S^y_{\text{Mn}}) - J_z S^z_{\text{Re}}S^z_{\text{Mn}}$$

INTRODUCTION

A great deal of activity involving the magnetic properties of transition metal polynuclear complexes has been observed in the past two decades: fascinating results have been obtained including spin crossover,[1] photomagnetism,[2] and single molecule magnetism.[3] The field of molecular magnetism (MM) has expanded into numerous new scientific and technological areas related to nanomagnetism and medicine, due to the perspective of using the above systems as constituents in spintronics, in quantum computers,[4] and as new theragnostic agents in medicine.[5] Single molecular magnetism, a significant domain of MM, covers the design and study of well-isolated paramagnetic molecules or one-dimensional polymers comprising magnetic tectons, named single-molecule magnets (SMMs)[6] and single-chain magnets (SCMs),[7] respectively. These systems can be blocked at low temperature in a well-defined magnetic state due to high anisotropy barriers. A great challenge is to design SMMs and SCMs with higher blocking temperatures (T_b). An important strategy to achieve this goal is to increase the magnetic anisotropy[8] that originates from both single-ion zero field splitting (ZFS) anisotropy of high-spin magnetic centers having $S \geq 1$ and anisotropic pair-spin coupling. Magnetic anisotropy of SMMs based on 3d metal ions is normally associated with the ZFS energy of individual high-spin magnetic centers. Since ZFS is only a second-order effect with respect to spin−orbit coupling (SOC), it generally leads to a small magnetic anisotropy.[9] Larger magnetic anisotropy could be obtained by using magnetic centers with unquenched orbital momentum (first-order effect), such as lanthanide ions and orbitally degenerate transition metal ions. In recent years, lanthanide-

Received: May 28, 2014
Published: September 24, 2014

based SMMs and SCMs have attracted considerable interest.[10−12] Very strong single-ion magnetic anisotropy and large magnetic momentum of lanthanide (Ln) ions are very efficient in increasing the molecular magnetic anisotropy of spin clusters and spin chains. Some of the lanthanide SMMs exhibit unusually high spin-reversal barriers and blocking temperature.[11] Recently it has been shown that the N_2^{3-} radical bridge can strongly couple two anisotropic Ln ions (Dy^{III} and Tb^{III}) resulting in small dinuclear lanthanide SMMs with a record blocking temperature.[13] However, Ln ions have a disadvantage of very weak spin coupling with other spin carriers due to extremely localized character of 4f electrons.[10−12] From this viewpoint, the use of orbitally degenerate 4d and 5d complexes with unquenched orbital momentum provides an attractive alternative way in engineering of exchange-coupled polynuclear complexes with slow relaxation of magnetization.[8a,b,c,14] It is important to point out that in these systems the origin of magnetic anisotropy is distinct from that in SMMs based on high-spin 3d ions since the low-spin ($S = {}^1/_2$) 4d or 5d magnetic centers have no ZFS effect requiring $S > {}^1/_2$. This means that the overall magnetic anisotropy originates largely from anisotropic pair-spin coupling rather than from single-center ZFS effect. High energy and diffuse 4d and 5d magnetic orbitals provide stronger exchange coupling to neighboring ions required for high T_b. Theoretical expectations,[8a,b,c] recently confirmed by experimental studies,[14−16] predict that orbitally degenerate cyanometallates of 4d (Mo^{III}, Ru^{III}) and 5d (Re^{IV}, Os^{III}) are the most promising systems to obtain effective and highly anisotropic magnetic exchange interactions between spin carriers in molecular clusters.

In the past few years a series of SMMs and SCMs[16−21] based on some of these highly anisotropic complex ions were synthesized and studied. Among them, SMMs based on orbitally degenerate $[Re^{IV}(CN)_7]^{3-}$ and $[Mo^{III}(CN)_7]^{4-}$ pentagonal bipyramidal complexes are of particular interest, namely, a pentanuclear cross-like $[(PY5Me_2)_4Mn_4Re(CN)_7]^{4+}$ complex ($Re^{IV}Mn^{II}_4$)[17a] and a linear trinuclear $[Mn(L_{N5Me})(H_2O)]_2[MoCN)_7]\cdot 6H_2O$ complex ($Mn^{II}-Mo^{III}-Mn^{II}$ or $MoMn_2$).[16] Despite the absence of single-ion ZFS anisotropy on the Mn^{II}, Re^{IV}, and Mo^{III} metal ions, these compounds exhibit a distinct SMM behavior with high values of energy barrier, largest among cyano-bridged SMMs, 33 and 40.5 cm^{-1} for $ReMn_4$ and in $MoMn_2$, respectively. Moreover, SMM characteristics of a small (only trinuclear) $MoMn_2$ cluster with a small ground-state spin $S = {}^9/_2$ (U_{eff} = 40.5 cm^{-1} and T_b = 3.2 K) are the same as those of the well-known $Mn_{12}Ac$ cluster (U_{eff} = 45 cm^{-1} and T_b = 3 K) with 12 magnetic ions and S = 10 ground-state spin.[16] These findings evidence the efficiency of orbitally degenerate 4d and 5d building blocks in designing high-temperature SMMs. In addition, two SMM compounds involving $[Ru^{III}(CN)_6]^{3-}$ and $[Os^{III}(CN)_6]^{3-}$ orbitally degenerate complexes with formula $(NEt_4)[Mn_2(5\text{-}Brsalen)_2(MeOH)_2\ M(CN)_6]$ display slow magnetization relaxation; they are part of a family of cyanide-bridged trinuclear clusters.[21a−e] All of these molecular clusters include Schiff base (SB) complexes of anisotropic 3d metal ion, Mn^{III}, a binuclear homometallic compound of the last possessing itself a SMM behavior.[22] Combination of two different types of anisotropic complexes has proven to be a successful approach for the design of SMMs[21a−e] and SCMs.[21f,g]

In this Article we have intended to extend this synthetic approach by incorporation of magnetically anisotropic, orbitally degenerate $[Mo^{III}(CN)_7]^{4-}$ and $[Re^{IV}(CN)_7]^{3-}$ anions as metalloligands for $[Mn^{III}SB]^+$ cations with the aim to obtain new heterobimetallic low-dimensional materials with high magnetic anisotropy. However, if during the synthesis of heterobimetallic compounds comprising Mo^{III} and Mn^{II}, a reduction[23] of $[Mo(CN)_7]^{4-}$ by Mn^{II} ion was not observed; then, in the case of rhenium the same reactions led to a 3D framework $[fac\text{-}Mn(H_2O)_3][cis\text{-}Mn(H_2O)_2][Re(CN)_7]\cdot 3H_2O$[24] in which the cyanometallate had spontaneously reduced to a diamagnetic species $[Re^{III}(CN)_7]^{4-}$. Moreover, the oxidation properties of $[Re(CN)_7]^{3-}$ have to be considered when a complex of Mn^{II} with pentacoordinated polypyridyl ligands is used as a partner.[17a] Thus, we propose the use of Mn^{III} complexes to enhance the stability of the final bimetallic compounds and to avoid a reduction process of Re^{IV}. In consideration of all forenamed features, the complex of SB, *N*,*N*′-ethylenebis(acetylacetoneimine) (H_2acacen), $[Mn^{III}(acacen)]^+$, was chosen as a partner for $[Re(CN)_7]^{3-}$ (see Scheme 1). It is worth noting that, by a combination of

Scheme 1

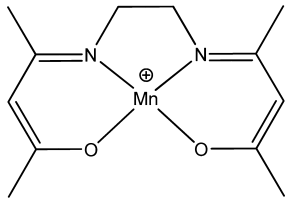

$[Mn(acacen)]^+$ with an iron cyanometallate, a row of heterobimetallic coordination compounds of different dimensionality (0D, 1D, and 2D) were obtained earlier, just varying the solvents and heating regime.[25] Unfortunately, all our attempts to obtain molecular or chain Re−Mn complexes failed, since, despite all synthetic condition variations, a neutral framework, $[Mn(acacen)]_3[Re(CN)_7]$ (**1**), was the only crystalline product. This compound is remarkable since it is a unique 3D coordination polymer among the $Mn^{III}SB$ complexes linked by homoleptic cyanometallates.

In this Article, we present the synthesis, crystal structure, and a magnetic study of both on powder and a single crystal of compound **1**. Some theoretical insight into the origin of magnetic anisotropy of **1** is also provided. We demonstrate that its unusual magnetic behavior results from a complicated interplay of Re−Mn anisotropic spin coupling and ZFS effect of Mn^{III} ions with a noncollinear orientation of the local magnetic axes in the 3D cyano-bridged network. A theoretical model of anisotropic spin coupling between orbitally degenerate $[Re^{IV}(CN)_7]^{3-}$ complexes and attached Mn^{III} ions is developed, and specific microscopic mechanisms of highly anisotropic spin coupling in $Re^{IV}-CN-Mn^{III}$ linkages in **1** are analyzed in detail.

EXPERIMENTAL SECTION

Materials. All chemicals and solvents employed for the syntheses were of analytical grade and used as received without further purification. $(Bu_4N)_3[Re(CN)_7]$[24] and [Mn(acacen)Cl][26] were synthesized according to literature procedures. H_2acacen was obtained by direct condensation of the molecular components.

Synthesis of $[Mn(acacen)]_3[Re(CN)_7]$, 1. A solution of $(Bu_4N)_3[Re(CN)_7]$ (45.6 mg, 0.0416 mmol) in 1.5 mL of methanol was added to a solution of [Mn(acacen)Cl] (39.5 mg, 0.1248 mmol) in 1.5 mL of CH_3OH. The black polycrystalline material was formed after reducing the reaction mixture volume up to 1 mL by heating. The solid was

dx.doi.org/10.1021/ic501247x | Inorg. Chem. 2014, 53, 10217−10231

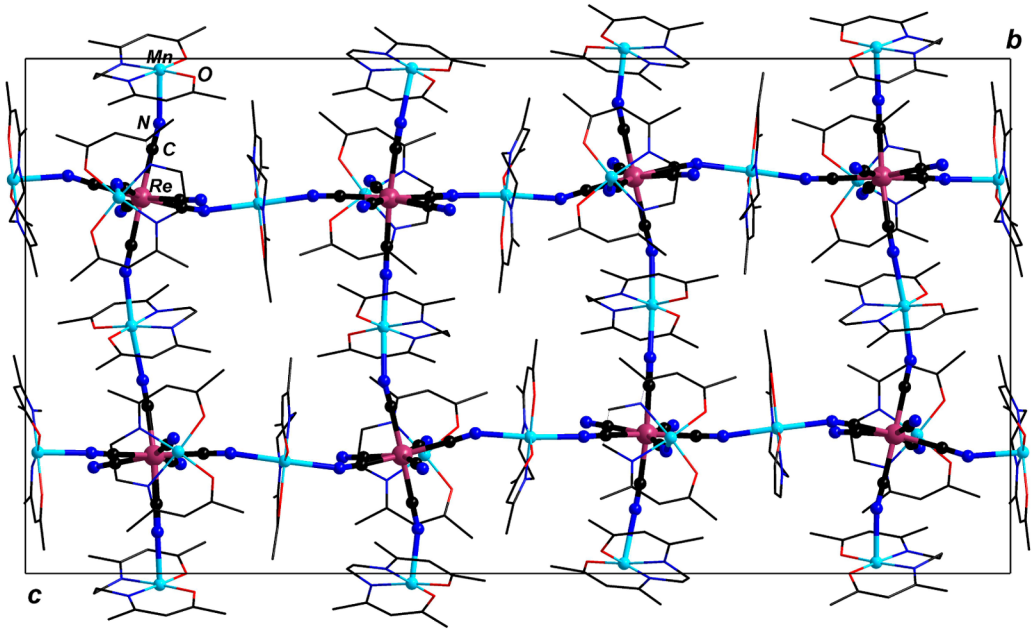

Figure 1. Unit cell of **1** projected on the *bc* plane. The apical axes of $[Re(CN)_7]^{3-}$ complexes (slightly distorted pentagonal bipyramids) are mainly oriented along the *b* axis, suggesting that *b* is the easy magnetic axis (see in the text).

separated by filtration, washed with 2 mL of CH_2Cl_2, 2 mL of 2-propanol, and twice by 1 mL of ether, and dried in air. Yield 42.5 mg (90%). Anal. Calcd (%) for $C_{43}H_{54}Mn_3N_{13}O_6Re$ (M =1200.01 g/mol): C, 42.99; H, 4.53; N, 15.17. Found: C, 43.07; H, 4.48; N, 15.21. FT-IR bands (KBr, cm^{-1}): ν(C≡N) 2128s, 2090.5s, 2045sh, ν(C═N) 1597, ν(C−OPhenolic) 1516.

Physical Measurements. The Fourier transform infrared spectra were recorded in the range 4000−370 cm^{-1} on a Scimitar FTS 2000 IR spectrophotometer with solid KBr pellets. C, H, and N microanalyses were carried out with a Euro-Vector 3000 elemental analyzer. Magnetic susceptibility data for bulk powder sample (17.05 mg) in Teflon homemade sample holder were collected over a 2−300 K temperature range using a MPMS SQUID magnetometer. The raw data were corrected for the sample holder and for the diamagnetic contributions of the constituents by using diamagnetic corrections and Pascal's constants.[27]

Low-temperature (below 2 K) magnetic measurements and ac susceptibility were performed on a powder and single crystal sample of **1** with SQUID magnetometers equipped with dilution refrigerators developed at the Institut Néel−CNRS, France.

Crystallographic Data Collection and Structure Refinement. Diffraction data for **1** were collected on a Bruker X8Apex CCD diffractometer with Mo Kα radiation (λ = 0.710 73 Å) using π and ω scans of narrow (0.5°) frames. Data collection, frame integration, and data processing were performed with the use of the APEX2 and SAINT program packages.[28b] The absorption correction (μ = 3.309 mm^{-1}) was applied on the basis of the intensities of equivalent reflections with the use of the SADABS program.[28b] The structure was solved by direct methods and refined anisotropically (except for the hydrogens atoms) by the full-matrix least-squares method using the SHELX-97 program package.[28a] Hydrogen atoms were refined in geometrically calculated positions. Single crystals of **1** were obtained by slow diffusion of Et_2O in CH_2Cl_2 solution, $C_{43}H_{54}Mn_3N_{13}O_6Re$, crystal size 0.73 × 0.12 × 0.03 mm^3 (dark plate), monoclinic, space group $P2_1/n$, a = 10.6492(3) Å, b = 21.8027(5) Å, c = 41.839(1) Å, β = 92.570(1)°, V = 9704.5(4) $Å^3$, d_{calc} = 1.643 g/cm^3, R1 = 0.0564, wR2 = 0.0996 Z = 8, T = 150 K. Powder diffraction investigations were performed at room temperature using an Expert-Pro powder diffractometer with Cu Kα radiation.

RESULTS

Synthesis of $[Mn(acacen)]_3[Re(CN)_7]$, 1. Heating of the methanol solution containing a Schiff base complex [Mn(acacen)Cl] and *n*-tetrabutylammonium heptacyanorhenate(IV) results in a precipitation of the polycrystalline 3D coordination framework **1**. In its IR spectrum (Figure S1 in the Supporting Information (SI)) a very strong ν_{CN} band composed of two partially resolved peaks with frequencies of 2128, 2090.8 cm^{-1} and a shoulder at 2045 cm^{-1} appear for **1**, differing substantially from 2114 and 2073.5 cm^{-1} characteristic for $(n\text{-}Bu_4N)_3[Re(CN)_7]$.[24] Note that the lower frequency peaks are close to 2097 and 2031 cm^{-1}, the values found for those in $[(PY_5Me_2)_4Mn_4Re(CN)_7](PF_6)_5\cdot 10H_2O$,[17a] pentanuclear molecule containing four bridging and three terminal CN^- groups. The presence of a third higher frequency peak can be explained by less symmetric arrangement of bridging cyano groups around the rhenium center compared to those in Re−Mn pentanuclear molecule.[17a]All attempts to obtain low-dimensional heterobimetallic coordination compounds failed despite a variation of ingredient proportions, solvents, and reaction conditions. In contrast to a combination of $[Mn(acacen)]^+$ with $[Fe(CN)_5NO]^{2-}$ recently described,[25] in all cases the rectangular dark crystals of **1** were obtained, the highest yield being achieved with the Mn:Re ratio of 3:1.

Crystal Structure. The X-ray crystal structure of **1** revealed a three-dimensional, charge-neutral network composed of $[Mn(acacen)]^+$ cations and $[Re(CN)_7]^{3-}$ anions (Figures 1 and 2), a crystallographically independent unit containing six manganese and two rhenium centers. Each Mn^{3+} ion has a distorted octahedral environment composed of two O and two N atoms of one tetradentate $acacen^{2-}$ ligand in equatorial plane, and two N atoms of CN bridges from $[Re(CN)_7]^{3-}$ ions in axial positions. The Mn−O and Mn−N_{SB} distances are in the range 1.891(4)−1.915(4) Å (average 1.904(8) Å) and 1.955(5)−1.987(5) Å (average 1.974(9) Å) correspondingly. The Mn−N_{CN} distances being in the range 2.297(5)−2.388(5) Å are typical for Jahn−Teller distorted Mn^{III} complexes. Each

dx.doi.org/10.1021/ic501247x | Inorg. Chem. 2014, 53, 10217−10231

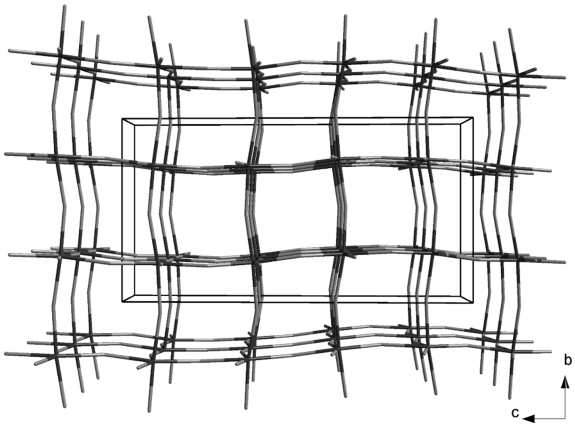

Figure 2. Schematic presentation of the 3D network with distorted cubic topology in **1**.

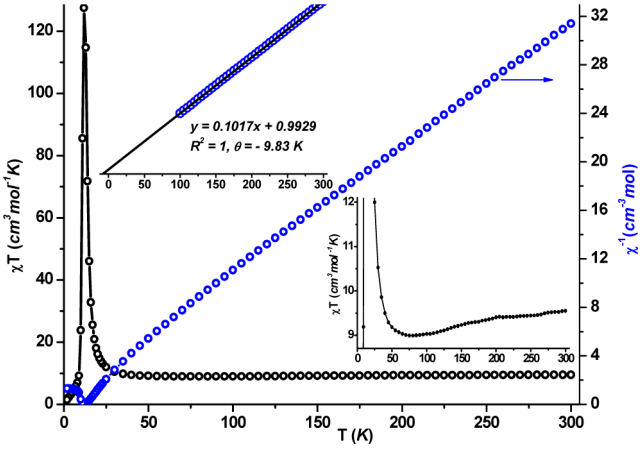

Figure 3. Temperature dependence of χT (black, solid line guides for eyes) and χ^{-1} (blue) for 1 at H = 5 kOe.

Re ion coordinates seven C atoms of CN ligands in a distorted pentagonal bipyramid. In fact, $[Re(CN)_7]^{3-}$ is much less distorted than its isoelectronic counterpart, $[Mo(CN)_7]^{4-}$.[23c] The Re−C distances are in the range 2.061(5)−2.144(5) Å, average 2.106(19) Å, comparable to those observed for $(Bu_4N)_3[Re(CN)_7]$[24] (2.064(10)−2.123(11) Å). Six CN ligands of $[Re(CN)_7]^{3-}$ ion connect to six $[Mn(acacen)]^+$ units forming a 3D network with distorted cubic topology (Figure 2). It should be noted that such framework organization of **1** is a unique example of 3D coordination heterobimetallic polymer constructed from a $[Mn^{III}SB]^+$ complex and a homoleptic cyanometallate. It could be explained by a combination of the compactness of the $[Mn(acacen)]^+$ ion in contrast with manganese(III) complexes of salen-type ligands, and a larger size of the 5d metal cyanide complex comparatively with 3d metal cyanides as well as elongated Mn−N_{CN} distances due to Jahn−Teller distortion. It is also probable that pentagonal bipyramidal arrangement of the metalloligand $[Re(CN)_7]^{3-}$ is favorable for the formation of 3D polymer; in any case there are not published examples of related bimetallic compounds based on octahedral cyanometallates.

For further interpretation of the magnetic properties it is important to note that a powder XRD spectrum corresponds perfectly to one calculated from SCXRD data, Supporting Information Figure S2. Practically all single crystals of **1** have the same form (rectangular plate, see Supporting Information Figure S3).

Magnetic Properties of Powder Sample. In this section we report experimental magnetic data of **1** followed by minor preliminary comments. More detailed discussion of magnetic behavior is provided below, after a theoretical section, in which highly anisotropic spin coupling between Re^{IV} and Mn^{III} ions is analyzed in terms of a microscopic model. The high-temperature dc susceptibility of a powder sample was measured in an applied field of 5 kOe, shown in Figure 3 as χT versus T and $1/\chi$ versus T plots. At 300 K, the observed χT value 9.55 is very close to 9.51 cm^3 K mol^{-1} expected for three Mn^{III} (S = 2) and one Re^{IV} ($S = {}^1/_2$, g = 2.33)[23] noninteracting spin carriers. Starting from room temperature, χT at first decreases slightly, and reaches a shallow minimum of 9 cm^3 K mol^{-1} at 80 K (Figure 3, down inset). This behavior of χT is characteristic of antiferromagnetic interactions between the Mn^{III} and Re^{IV} ions; the origin of a minimum is discussed below more quantitatively in terms of a theoretical model. The analysis of the $1/\chi$ versus T curve shows that, from 300 to 100 K, χ obeys a Curie−Weiss law with Θ = −9.8 K and C = 9.86 cm^3 K mol^{-1} (Figure 3, upper inset), confirming the antiferromagnetic character of exchange couplings in this compound. Below 50 K, χT increases and finally reaches a sharp maximum at 13 K suggesting a magnetic phase transition in a 3D network. A similar behavior has earlier been observed in related Mn^{II}−$[Mo^{III}(CN)_7]$ frameworks, containing the isoelectronic pentagonal bipyramidal $[Mo^{III}(CN)_7]^{4-}$ unit.[23e] Even if such a behavior is reminiscent of that of ferromagnetic compounds, the underlying reason is much more complicated and will be discussed later.

The ac susceptibility of the sample taken in a field of 1 Oe for various frequencies in the vicinity of the maximum is shown in Figure 4. There is no frequency dependence in the ac data. In addition, the imaginary part of the susceptibility χ'' is very small, and shows only a small onset like anomaly just at the peak in χ'. This behavior suggests a sharp phase transition at 13 K. The dc susceptibility taken in a field of 100 Oe is also shown in the figure. The value of susceptibility is very large at the maximum, but no spontaneous moment was detected below

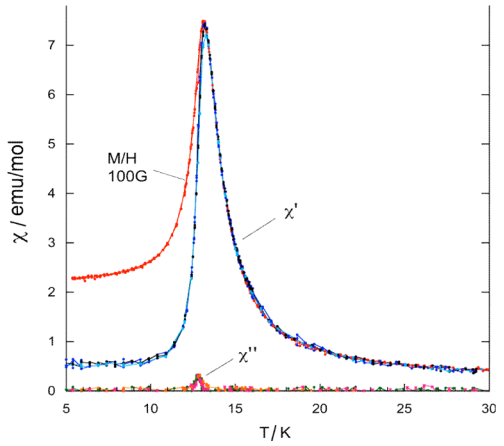

Figure 4. Direct current susceptibility M/H taken in a field of 100 Oe and the real and imaginary part of the ac susceptibility taken in a field of 1 Oe at 0.57, 5.7, and 57 Hz vs temperature for a powder sample. There is almost no dispersion in χ, and the imaginary part shows only a very small onset like anomaly at the peak, indicating the presence of a phase transition.

dx.doi.org/10.1021/ic501247x | Inorg. Chem. 2014, 53, 10217−10231

the transition since the initial slope of the M versus H curves is not constant below the peak in the susceptibility as would be expected for a ferromagnetic transition. In fact the slope decreases as can be seen in Figure 5. Thus, we can rule out a

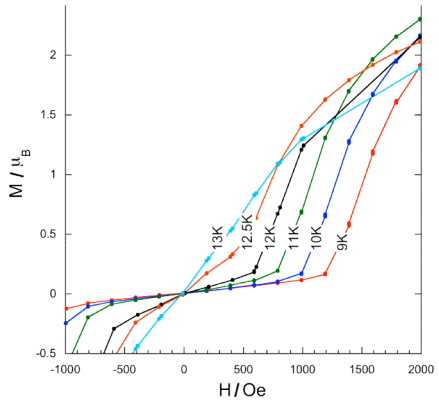

Figure 5. M vs H at various constant temperatures near T_N measured on a powder sample. The behavior of M below 13 K is reminiscent of a metamagnetic transition from an antiferromagnetic state to a polarized state.

ferromagnetic transition. Supporting Information Figure S4 indicates that at 2 K a metamagnetic transition occurs in the field about 5 kOe. This behavior appears at temperatures below the maximum in susceptibility shown in Figure 4, as evidenced by M versus H curves measured at various constant temperatures in Figure 5. These results indicate that the maximum of susceptibility can be identified as the Néel temperature T_N= 13 K, below which the system exhibits a metamagnetic behavior with some field-induced magnetic transitions.

Notwithstanding the lack of ferromagnetic order, hysteresis was observed at low temperatures measured on a powder sample at 200 mK, Figure 6. The blue data points are the initial

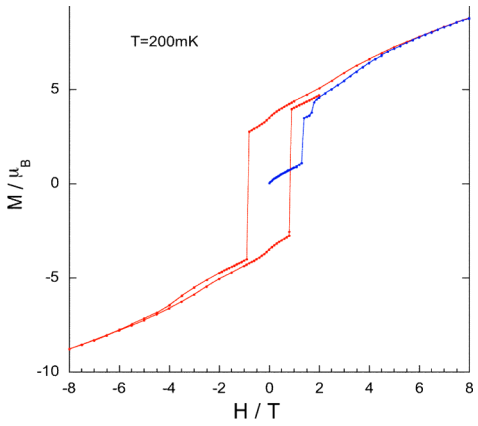

Figure 6. Hysteresis cycle measured on a powder sample at 200 mK. The blue data points are the initial magnetization from the zero field cooled state.

magnetization curve after first zero field cooling the sample from above the transition temperature. As can be seen, the magnetization jumps, or avalanches when the field reaches a critical value near 1.3 T. Another smaller jump occurs near 2 T (20 kOe), and the hysteresis is closed only when the field is greater than 4 T (40 kOe). The full hysteresis cycle shows a very large coercive field of approximately 1 T or 10 kOe, attesting to a very large anisotropy in this sample. Furthermore, the sample does not saturate at 200 mK even in fields up to 8 T (80 kOe), and exhibits a linear dependence at high field which is typical for strongly anisotropic systems. The maximum value of M obtained is approximately 8.8 μ_B far from the theoretical expectation (13 μ_B for ferromagnetic coupling between the Mn^{III} and Re^{IV} ions, and 11 μ_B for antiferromagnetic coupling). Note also that, at H = 0, the magnetization does not reach $^1/_2$ of the saturation value, as might be expected for a powder sample with a simple uniaxial anisotropy, but is significantly smaller, approximately 3.6 μ_B. This could imply that the spins are canted.

In summary, this powder study shows that in **1** there is an antiferromagnetic ordering occurring at a Néel temperature of 13 K. In addition, a strong anisotropy is present, and the analysis of the M versus H curves indicates that the ordered magnetic structure may be canted. This suggests a complicated magnetic structure, which is analyzed in more detail later in terms of a competition between Re−Mn anisotropic antiferromagnetic spin coupling and single-ion magnetic anisotropy of Mn^{III} ions in a low-symmetry bimetallic 3D network of **1** (see the Discussion section).

Magnetic Properties of a Single Crystal. In order to get insight into the expected anisotropic behavior of the material, a preliminary study was performed on a single crystal. All crystals of **1** have a form of rectangular plate with a long dimension perpendicular to the (100) plane and corresponding to the c axis, the medium dimension along b axis ($\perp$(010) plane), and the shortest dimension along a axis perpendicular to the surface of the plate (001), see Supporting Information Figure S3. For the measurements we have chosen the largest crystal of mass 0.000 07 ± 0.000 03 g with dimensions approximately 1 × 0.7 × 0.03 mm^3 thick along the three crystallographic directions. Unfortunately due to the large uncertainties in measuring of the sample mass (related to difficulties gluing the sample on a small Cu holder), we present the data in arbitrary units, and focus on the relative measurements between the different directions of the crystal.

In Figure 7 we present a plot of the dc susceptibility, measured along the three principle directions of the crystal.

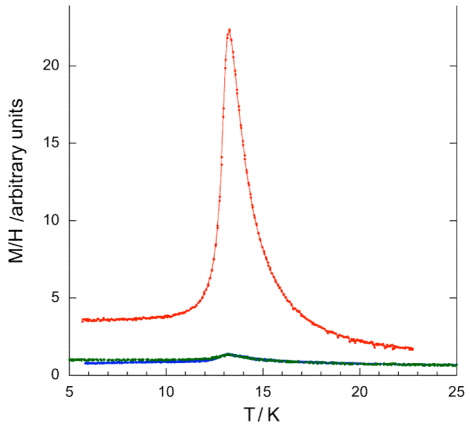

Figure 7. M vs H measured along the three different crystallographic directions. The red indicates b direction $\perp$(010), and the field was 100 Oe. The green curve along with a axis $\perp$(001) was measured in a 500 Oe field, and the blue shows c axis $\perp$(100) plane direction measured in a 1000 Oe field.

dx.doi.org/10.1021/ic501247x | Inorg. Chem. 2014, 53, 10217−10231

The easy magnetization axis is along the b direction ($\perp$010), and the susceptibility is more than an order of magnitude larger than along the other two directions. In Figure 8 we show

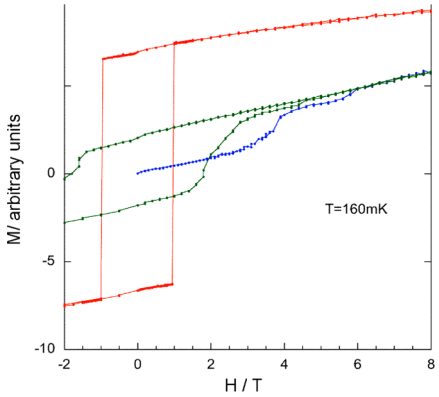

Figure 8. Hysteresis loops measured along the 010 axis (red) and along the 100 axis (green) and the initial magnetization along the 100 axis (blue). The data were taken at 160 mK.

hysteresis loops measured at 160 mK along b ($\perp$010) and c ($\perp$100) directions, as well the initial magnetization curve for the c direction. For the initial magnetization curve two fields may be identified with changes in the magnetization at 4 and 6 T, which are rather large. On the other hand, for the b ($\perp$010) direction, a sharp jump in the magnetization occurs at 1 T. The easy axis of magnetization, b, corresponds to the preferable orientation of the apical axes of the pentagonal bipyramids of $[Re(CN)_7]^{3-}$ (Figures 1 and 2), while the second direction is in the equatorial plane (a or c), Supporting Information Figure S3a. Note that, even along the easy axis, the magnetization still has not saturated at 8 T (80 kOe) and 160 mK, indicating that the spins are not perfectly aligned along this direction, and provide further evidence that they may be canting.

In summary, the magnetic study shows that **1** undergoes an antiferromagnetic ordering of a complicated character below Néel temperature of 13 K. This system exhibits a metamagnetic behavior and strong magnetic anisotropy similar to those observed in related 3D polymer Mn^{II}–$[Mo(CN)_7]^{4-}$ systems. Below we show that these unusual magnetic properties are due to an extremely sophisticated interplay of anisotropic spin coupling of Mn^{III}–CN–Re^{IV} linkages and single-ion ZFS anisotropy of $[Mn^{III}SB]^+$ complexes in the 3D network of **1**.

THEORY

Analysis of Anisotropic Spin Coupling of Re–CN–Mn Linkages in 1. In this section we develop a microscopic theory describing anisotropic spin coupling between orbitally degenerate $[Re^{IV}(CN)_7]^{3-}$ complexes and high-spin Mn^{III} ions in cyano-bridged 3D network of **1**. We provide a theoretical insight into the origin of anisotropic spin coupling in Re–CN–Mn linkages with real (distorted) structure of **1** (Figures 1 and 2). As has been previously shown in terms of the superexchange theory for the isoelectronic $[Mo^{III}(CN)_7]^{4-}$ complex with idealized pentagonal bipyramidal structure, anisotropic spin coupling between $[Mo^{III}(CN)_7]^{4-}$ and high-spin Mn^{II} ions ($S = {}^5/_2$) connected via cyano groups is described by a pure Ising-type spin Hamiltonian $-J_z S^z_{Mn} S^z_{Mo}$ for the apical Mo^{III}–CN–Mn^{II} pairs and by $-J_{xy}(S^x_{Mn}S^x_{Mo} + S^y_{Mn}S^y_{Mo}) - J_z S^z_{Mn}S^z_{Mo}$, a uniaxial anisotropic spin coupling for the equatorial pairs.[8b] Herein we show that for the regular (D_{5h} symmetry) or slightly distorted pentagonal bipyramidal structure of the $[Re(CN)_7]^{3-}$ unit the spin coupling in low-symmetry (bent and distorted) Re–CN–Mn fragmentes in **1** (both apical and equatorial) is also described by $-J_{xy}(S^x_{Mn}S^x_{Re} + S^y_{Mn}S^y_{Re}) - J_z S^z_{Mn}S^z_{Re}$, an uniaxial anisotropic spin Hamiltonian, irrespective of the actual local symmetry of linked $[Mn^{III}SB]^+$ ions. This implies that the

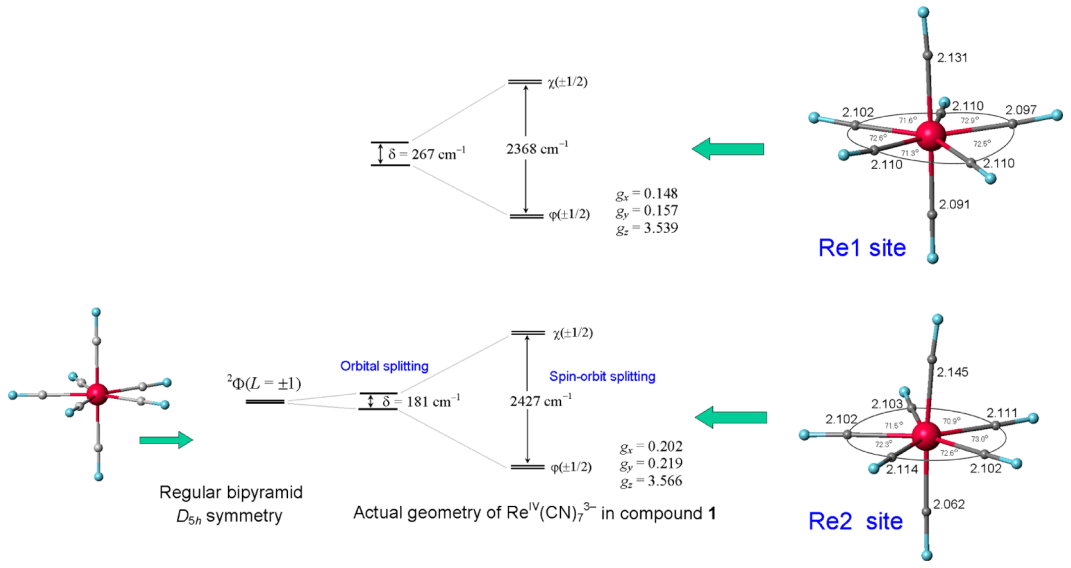

Figure 9. Orbital splitting energy δ and SOC energy of the ground orbital doublet $^2\Phi(L = \pm1)$ of pentagonal-pyramidal $[Re(CN)_7]^{3-}$ units for Re1 and Re2 sites in **1**. In the regular pentagonal symmetry (D_{5h}) of $[Re(CN)_7]^{3-}$, the ground orbital doublet $^2\Phi(L = \pm1)$ is strictly degenerate. Distortions split the $^2\Phi(L = \pm1)$ doublet into two orbital components by the energy δ. SOC of Re (with ζ_{Re}= 2400 cm^{-1}) further splits the orbital doublet $^2\Phi(L = \pm1)$ into two magnetically anisotropic Kramers doublets, the ground $\varphi(\pm{}^1/_2)$ and excited $\chi(\pm{}^1/_2)$ Kramers doublet; calculated anisotropic g-tensor components of the Re1 and Re2 sites are indicated. The δ is much smaller than the spin–orbit splitting energy (see Supporting Information for detail). This implies that the ground-state orbital momentum of Re1 and Re2 sites remains unquenched. Selected Re–C distances (in Å) and bonds angles of distorted $[Re(CN)_7]^{3-}$ anions are indicated.

dx.doi.org/10.1021/ic501247x | Inorg. Chem. 2014, 53, 10217–10231

symmetry lowering of the Re−CN−Mn groups does not destroy the uniaxial symmetry of the spin Hamiltonian as long as the $[Re(CN)_7]^{3-}$ pentagonal bipyramid remains undistorted or slightly distorted. Then we perform numerical microscopic calculations of anisotropic exchange parameters J_z and J_{xy} for all Re−CN−Mn linkages in the real low-symmetry structure of **1** in terms of a many-electron superexchange theory.

Electronic Structure of $[Re(CN)_7]^{3-}$. First we outline the electronic structure and single-center magnetic characteristics of the orbitally degenerate $[Re(CN)_7]^{3-}$ units in **1** (Figure 9). For a Re^{IV} ion in the regular pentagonal-bipyramidal (D_{5h}) polyhedron, the ground state is orbitally degenerate: when spin−orbit coupling is neglected, the ground energy level is represented by a low-spin orbital doublet $^2\Phi_\pm = {}^2\Phi(L= \pm1)$, whose two ± components correspond to the $M_L = \pm1$ projection of the unquenched orbital momentum L on the polar z-axis of the $[Re(CN)_7]^{3-}$ bipyramid. These components are described by the degenerate ground electronic configurations $(d_{+1})^2(d_{-1})^1$ and $(d_{-1})^2(d_{+1})^1$ involving complex d orbitals $d_{\pm1} = (d_{xz} \pm id_{yz})/\sqrt{2}$ with definite values of the projection of L ($m_l = \pm1$) on the z axis of the pentagonal bipyramid. Alternatively, they can also be described as two real components represented by the configurations $(d_{xz})^2(d_{yz})^1$ and $(d_{yz})^2(d_{xz})^1$. SOC of Re^{IV} splits the orbital doublet $^2\Phi_\pm$ into the ground $\varphi(\pm^1/_2)$ and excited $\chi(\pm^1/_2)$ Kramers doublets. Two components of the ground Kramers doublet $\varphi(\pm^1/_2)$ are well-described by the electronic configurations $(d_{+1})^2(d_{-1})\uparrow$ and $(d_{-1})^2(d_{+1})\downarrow$;[8b] admixture of excited $5d^3$ ligand-field (LF) states is very small due to a very large energy gap between the ground state $^2\Phi_\pm$ and first excited LF state (around 20 000 cm^{-1}, as estimated from LF calculations). The ground Kramers doublet $\varphi(\pm^1/_2)$ has a highly anisotropic Ising-like g-tensor (such as g_z = 3.66 and $g_x = g_y$ =1.59)[24] and exhibits strongly anisotropic spin coupling with Mn^{III} ions bounded via CN^- groups (see below).

For a slightly distorted $[Re(CN)_7]^{3-}$ bipyramid, as is the case in **1**, this situation changes insignificantly: the orbital momentum of $[Re(CN)_7]^{3-}$ remains unquenched, and the ground-state wave functions are nearly the same as those in the regular D_{5h} polyhedron as long as the splitting energy of $^2\Phi_\pm$ is much less than the spin−orbit splitting energy ≈2400 cm^{-1} (see Supporting Information for more detail). Therefore, the use of the idealized D_{5h} geometry of $[Re(CN)_7]^{3-}$ is a good model approach in theoretical analysis of anisotropic spin coupling in compound **1**.

Origin of Strong Exchange Anisotropy in Re−CN−Mn Pairs. A Microscopy Theory. In order to elucidate in detail the origin of strong exchange anisotropy in bent Re−CN−Mn exchange-coupled pairs involving the orbitally degenerate $[Re(CN)_7]^{3-}$ complex, we first neglect SOC of the Re^{IV} center. This allows us to relate anisotropic exchange parameters J_{xy} and J_z associated with the ground Kramers doublet $\varphi(\pm^1/_2)$ with the orbital exchange parameters J_1 and J_2 associated with two individual orbital components $^2\Phi_{xz}$ and $^2\Phi_{yz}$ of the orbitally degenerate ground state $^2\Phi_\pm$ of $[Re(CN)_7]^{3-}$. With zero SOC for 5d electrons, the true total spin $S_{Re} = {}^1/_2$ of $[Re(CN)_7]^{3-}$ is decoupled with the unquenched orbital momentum L (represented by two projections $M_L = \pm1$ on the polar z-axis of the $[Re(CN)_7]^{3-}$ bipyramid), so the spin $S_{Re} = {}^1/_2$ becomes a good quantum number. In this case, the exchange spin Hamiltonian $\hat{H}$describes isotropic orbitally dependent spin coupling between the $^2\Phi_\pm$ orbital doublet of Re^{IV} and the spin $S_{Mn} = 2$ of the Mn^{III} center. In the general case, it can be written as

$$\hat{H} = \mathbf{A} + \mathbf{R}\mathbf{S}_{Re}\mathbf{S}_{Mn} \quad (1)$$

where $\mathbf{S}_{Re}$ and $\mathbf{S}_{Mn}$ are spin operators of Re and Mn; **A** and **R** are, respectively, spin independent and spin dependent orbital operators acting on the orbital variables only. In the basis set of two wave functions of the orbital doublet $^2\Phi$, the **A** and **R** orbital operators are written as a 2 × 2 matrix

$$\mathbf{A} = \begin{pmatrix} A_{11} & A_{12} \\ A_{21} & A_{22} \end{pmatrix} \text{ and } \mathbf{R} = \begin{pmatrix} J_{11} & J_{12} \\ J_{21} & J_{22} \end{pmatrix} \quad (2)$$

For the undistorted or slightly distorted $[Re(CN)_7]^{3-}$ polyhedron, the **R** matrix can be always reduced to a diagonal form by a canonical transformation of two wave functions $^2\Phi_+$ and $^2\Phi_-$ corresponding to a rotation of the coordinate frame (xyz) around the z-axis by certain angle φ. Omitting the spin-independent operator **A** (which has no influence on further calculations) we obtain

$$\hat{H} = \begin{pmatrix} J_1 & 0 \\ 0 & J_2 \end{pmatrix} \mathbf{S}_{Re}\mathbf{S}_{Mn} \quad (3)$$

where the orbital exchange parameters J_1 and J_2 refer, respectively, to the real wave functions $^2\Phi_{xz} = (d_{yz})^2(d_{xz})^1$ and $^2\Phi_{yz} = (d_{xz})^2(d_{yz})^1$ (more detailed calculations and comments are presented in Supporting Information).

Then, the SOC on Re^{IV} is switched on, and the effective spin Hamiltonian $\hat{H}_{eff}$ describing anisotropic spin coupling between the ground Kramers doublet $\varphi(\pm^1/_2)$ (corresponding to a fiction spin $S_{Re}(eff) = {}^1/_2$) is obtained by projection of the Hamiltonian in eq 3 onto the space of wave functions $|m, M_S\rangle = \varphi(m) \times |S_{Mn}, M_S\rangle$, where $m = \pm^1/_2$ is a projection of $S_{Re}(eff)$ on the polar z-axis of the bipyramid, $|S_{Mn}, M_S\rangle$ is the wave function of Mn^{III} with the spin projection M_S, and × stands for antisymmetrized product. The effective spin Hamiltonian $\hat{H}_{eff}$ is obtained in first-order perturbation theory by equating the matrix elements of H_{eff} and $\mathbf{R}\mathbf{S}_{Re}\mathbf{S}_{Mn}$ in the space of wave functions $|m, M_S\rangle$, $\langle m, M_S|\hat{H}_{eff}|m', M_S'\rangle = \langle m, M_S|\mathbf{R}\mathbf{S}_{Mo}\mathbf{S}_{Mn}|m', M_S'\rangle$. In terms of the Re and Mn spin operators, this set of matrix elements corresponds to a spin Hamiltonian

$$\hat{H}_{eff} = -J_{xy}(S^x_{Mn}S^x_{Re} + S^y_{Mn}S^y_{Re}) - J_zS^z_{Mn}S^z_{Re} \quad (4)$$

where $J_z = (J_1 + J_2)/2$, $J_{xy} = (J_1 - J_2)/2$, and $|J_1| \geq |J_2|$; note that J_z and J_{xy} have the same sign. This spin Hamiltonian exhibits several interesting features. Importantly, $\hat{H}_{eff}$ always has an uniaxial symmetry with the anisotropy z-axis parallel to the polar axis of the $[Re(CN)_7]^{3-}$ anion, regardless of the C−N−Mn bending angle and specific orientation of the connected Mn^{III} center with respect to the central $[Re(CN)_7]^{3-}$ unit, Figures 10−13. Note that this feature is a general property of undistorted orbitally degenerate $[Re(CN)_7]^{3-}$ complex originating exclusively from the D_{5h} symmetry and transformational properties of wave functions of the ground orbital doublet, regardless of the specific microscopic mechanism of Re−Mn anisotropic spin coupling.

The relation between the J_z and J_{xy} anisotropic exchange parameters in eq 4is different for the apical and equatorial positions of bound $[Mn^{III}acacen]^+$ units. For the apical positions both orbital exchange parameters are antiferromagnetic, $J_1 < 0$ and $J_2 < 0$; thus, according to the relations $J_z = (J_1 +$

dx.doi.org/10.1021/ic501247x | Inorg. Chem. 2014, 53, 10217−10231

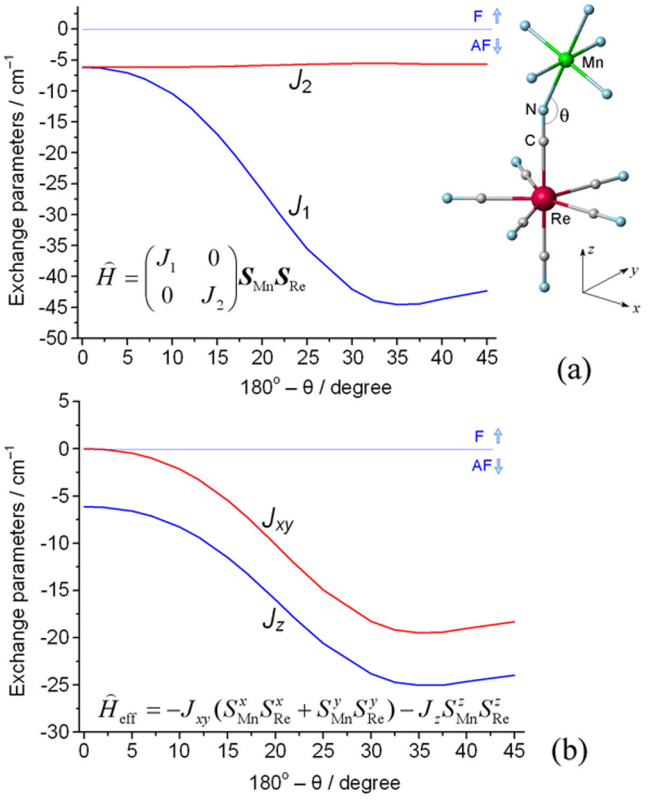

Figure 10. Calculated variation of exchange parameters vs the bending angle 180° − θ for the apical Re−CN−Mn pair: (a) variation of orbital parameters J_1 and J_2 in the orbitally dependent spin Hamiltonian in eq 3, (b) variation of anisotropic exchange parameters J_z, J_{xy} in the spin Hamiltonian in eq 4. Spin quantization axes x, y, and z are indicated. The MnN_4O_2 polyhedron (tetragonally elongated octahedron, D_{4h} symmetry; for simplicity, the difference between O and N atoms in MnN_4O_2 is not shown) rotates as a whole in the vertical zx plane around marked nitrogen atom. With the increasing bending angle, both the anisotropic exchange parameters J_z, J_{xy} increase, but the difference $J_z - J_{xy}$ remains nearly constant.

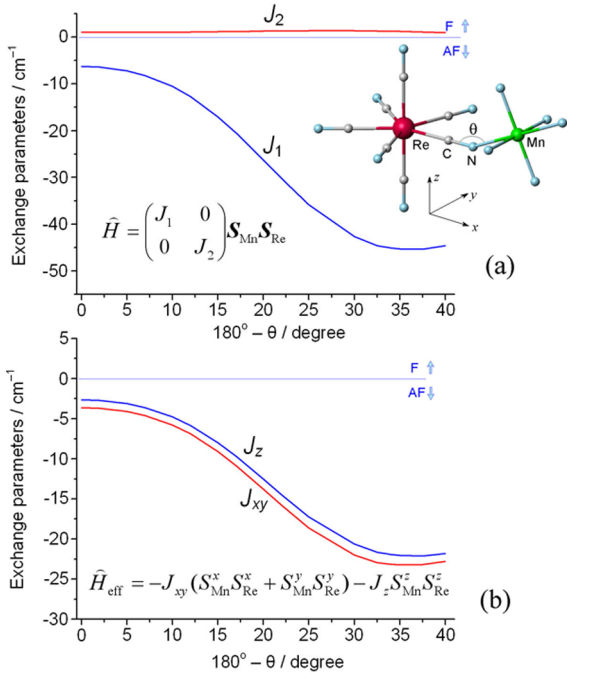

Figure 11. Exchange parameters vs bending angle 180° − θ dependence, calculated for the equatorial Re−CN−Mn pair: (a) variation of orbital exchange parameters J_1 and J_2, parameter J_2 is weakly ferromagnetic and nearly constant; (b) variation of anisotropic exchange parameters J_z and J_{xy}. Spin quantization axes x, y, and z are indicated. The MnN_4O_2 polyhedron rotates as a whole in the vertical zx plane around marked nitrogen atom. In contrast to the apical pair, magnetic anisotropy has a xy-character, $|J_{xy}| > |J_z|$, though the whole spin coupling is nearly isotropic.

$J_2)/2$ and $J_{xy} = (J_1 - J_2)/2$, we have a z-character (Ising-like) of the exchange anisotropy, $J_z < 0$, $J_{xy} < 0$, and $|J_z| > |J_{xy}|$ (because $|J_1 + J_2| > |J_1 - J_2|$ for the same sign of the exchange parameters J_1 and J_2). Pure Ising-type $-J_z S^z_{Re}S^z_{Mo}$ occurs only for a linear apical Re−CN−Mn pair, where $J_1 = J_2$ is due to axial symmetry condition for the apical pair (Figure 9), just as obtained from earlier microscopic calculations for Mo^{III}−CN−Mn^{II} pairs in terms of the superexchange theory.[8b] Thus, any symmetry lowering of the apical Re−CN−Mn groups results only in the appearance of the transverse component J_{xy} in eq 4, but does not destroy the uniaxial symmetry of the anisotropic spin Hamiltonian in eq 4.

For the equatorial positions J_1 is antiferromagnetic ($J_1 < 0$), but J_2 is weakly ferromagnetic ($J_2 > 0$) due to orthogonality of the $5d_{yz}$(Re) magnetic orbital with respect to all 3d(Mn) orbitals; thus for equatorial Re−CN−Mn fragments we have an xy-character of the anisotropic spin coupling (eq 4) with $|J_z| < |J_{xy}|$. In the next section the anisotropic exchange parameters are analyzed in much more detail in terms of numerical superexchange calculations.

Calculation of Anisotropic Exchange Parameters. With this theoretical background, we now evaluate anisotropic exchange parameters J_z and J_{xy} for the Re−CN−Mn exchange-coupled pairs in **1**. We analyze the dependence of the J_z and J_{xy} parameters on the C−N−Mn bonding angle for the apical and equatorial Re−CN−Mn pairs in terms of a many-electron superexchange theory similar to that employed for the analysis of anisotropic spin coupling between Yb^{III} and Cr^{III} ions in a 4f−3d $YbCrBr_9^{3-}$ dimer.[29] Details of these superexchange calculations are reported in Supporting Information.

Using this approach, we analyze variation of the orbital (J_1, J_2,) and anisotropic (J_z, J_{xy}) exchange parameters with the increasing bending of the C−N−Mn unit for the apical and equatorial Re−CN−Mn pairs. In these calculations, we use an idealized (symmetrized) structure of $[Re(CN)_7]^{3-}$ and [Mn-(acacen)]$^+$ units: $[Re(CN)_7]^{3-}$ is regarded as a regular pentagonal bipyramid (D_{5h}), while the coordination polyhedron of the Jahn−Teller (JT) Mn^{III} ion corresponds to a tetragonally elongated MnN_4O_2 octahedron (D_{4h} symmetry) with two apical distances Mn−N = 2.33 Å and with four equatorial distances Mn−N = 1.92 Å (Figures 10−12); these distances approximately correspond to average atomic distances in 12 nonequivalent Re−CN−Mn pairs in the crystal structure of **1** (Table 1, Figures 1 and 13).

Calculated variation of the J_1 and J_2 parameters in the isotropic orbitally dependent spin Hamiltonian in eq 3 and J_z, J_{xy} parameters in eq 4 [which are related by $J_z = (J_1 + J_2)/2$ and $J_{xy} = (J_1 - J_2)/2$] is summarized graphically in Figures 10−12.

These calculations show that anisotropy of the spin coupling in $Re^{IV}(CN)_7^{3-}$-based molecular magnets is very sensitive to distortions in the Re−CN−Mn groups. Importantly, variation of the exchange parameters has a different character for the apical and equatorial pairs. For the apical pairs pure Ising-type

dx.doi.org/10.1021/ic501247x | Inorg. Chem. 2014, 53, 10217−10231

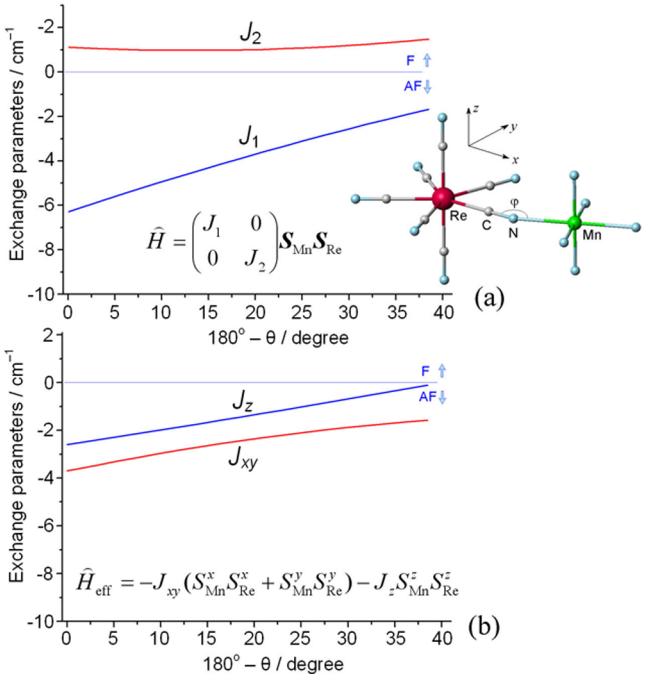

Figure 12. Exchange parameters vs azimuthal bending angle $180° - \varphi$ dependence calculated for the equatorial Re−CN−Mn pair: (a) variation of orbital exchange parameters J_1 and J_2, parameter J_2 is weakly ferromagnetic and is nearly constant; (b) variation of anisotropic exchange parameters J_z and J_{xy}. Spin quantization axes x, y, and z are indicated. The MnO_4N_2 polyhedron rotates as a whole in the horizontal xy plane around marked nitrogen atom. Magnetic anisotropy has a xy-character, $|J_{xy}| > |J_z|$, with small antiferromagnetic exchange parameters.

exchange anisotropy ($J_z < 0$ and $J_{xy} = 0$) occurs only for a strictly linear Re−CN−Mn group ($\theta = 180°$, Figure 10), as has previously been predicted.[8b] In this case, the antiferromagnetic parameter J_z is rather small ($J_z \sim -6$ cm^{-1}, Figure 10b). Note that J_z is always antiferromagnetic since $J_1 < 0$ and $J_2 < 0$ (Figure 10a). With the increasing bending angle ($180° - \theta$) in the polar Re−CN−Mn pair, the absolute value of the J_1 orbital parameter rapidly increases (to ~ -45 cm^{-1} at $180° - \theta \approx 35°$, Figure 10a) because of opening of a new superexchange pathway of mixed $\sigma\pi$-type due to nonorthogonality of $5d_{xz}$(Re) (π-type) and $3d_{z^2}$(Mn) (σ-type) magnetic orbitals. In contrast, J_2 orbital parameter remains nearly constant ($J_2 \approx -6$ cm^{-1}). As result, the absolute value of J_z and J_{xy} anisotropic exchange parameters rapidly increases, but the relative degree of the exchange anisotropy drops (i.e., $J_z/J_{xy} \approx 1$); note that both J_z and J_{xy} are antiferromagnetic, $|J_z| > |J_{xy}|$, and the difference $|J_z - J_{xy}|$ is nearly constant (Figure 10b).

In the equatorial pairs, variation of exchange parameters with the polar bending angle ($180° - \theta$) has a similar character to that for the apical pair except that the J_2 orbital parameters is now slightly ferromagnetic ($J_2 \sim +1$ cm^{-1}) due to orthogonality between the $5d_{yz}$(Re) orbital and all 3d(Mn) magnetic orbitals, Figure 11.

As a result, from equations $J_z = (J_1 + J_2)/2$ and $J_{xy} = (J_1 - J_2)/2$, we have a nearly isotropic spin coupling $J_z \approx J_{xy}$ with a small anisotropic component of xy-character (i.e., $|J_z| < |J_{xy}|$). In addition, our calculations indicate that azimuthal bending of equatorial Re−CN−Mn pairs ($180° - \varphi$) has a small influence on the exchange parameters, Figure 12.

With these results, we estimate anisotropic exchange parameters J_z and J_{xy} for all 12 nonequivalent Re−CN−Mn pairs in the crystal structure of **1**, Table 1. Because in the equatorial pairs exchange parameters depend not only on the absolute value of the C−N−Mn bonding angle but also on its polar θ and azimuthal φ components (along the z-axis and in the xy plane of $[Re(CN)_7]^{3-}$, respectively, Figures 11 and 12), we have estimated the θ and φ angles from the geometry analysis (Table 1). Using these angles in the idealized geometry of Re−CN−Mn bridging units, we obtain J_z and J_{xy} from superexchange calculations (see Supporting Information for more detail).

These theoretical results show that there is an extremely complicated interplay of anisotropic spin coupling between apical and equatorial Re−CN−Mn pairs in the framework of **1**. Although in all pairs the anisotropic spin Hamiltonian $\hat{H}_{eff} = -J_{xy}(S^x_{Mn}S^x_{Re} + S^y_{Mn}S^y_{Re}) - J_zS^z_{Mn}S^z_{Re}$ always has a uniaxial symmetry with the anisotropy z axis parallel to the polar axis of the $[Re(CN)_7]^{3-}$ bipyramid, anisotropic exchange parameters J_z and J_{xy} vary considerably from pair to pair. Exchange anisotropy for the apical pairs shows a pronounced Ising-like character ($|J_z| > |J_{xy}|$), while the spin coupling in equatorial pairs is close to be isotropic (with a small xy-component).

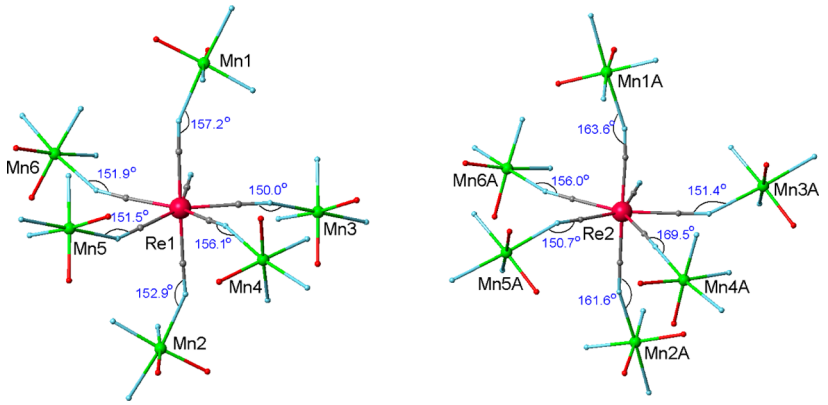

Figure 13. Local structure of 12 nonequivalent Re−CN−Mn exchange-coupled pairs in **1**. The C−N−Mn bonding angles are indicated; for each equatorial pair, the polar (θ, parallel to the polar z-axis of $Re(CN)_7$, Figures 10 and 11) and azimuthal (φ, in the equatorial xy plane, Figure 12) components of the C−N−Mn bonding angle are obtained from the geometry analysis. Selected atomic distances and θ and φ angles are presented in Table 1.

dx.doi.org/10.1021/ic501247x | Inorg. Chem. 2014, 53, 10217−10231

Table 1. Geometry Parameters of 12 Nonequivalent Re−CN−Mn Pairs in the Crystal Structure of 1 (Figure 13) and Calculated Anisotropic Exchange Parameters J_z and J_{xy}

Re−CN−Mn pair		atomic distances, Å			C−N−Mn bonding angles and their components, deg			exchange params, cm^{-1}	
Re center	Mn center	Re−C	C−N	N−Mn	$\angle_{iCNMn}$	θ	φ	J_z	J_{xy}
Re1	Mn1	2.132	1.124	2.334	157.2	157.2		−18.6	−12.9
Re1	Mn2	2.092	1.174	2.336	152.9	152.9		−23.1	−17.5
Re1	Mn3	2.110	1.156	2.336	150.0	169.1	153.2	−4.8	−5.8
Re1	Mn4	2.097	1.158	2.342	156.1	156.7	173.0	−16.0	−17.4
Re1	Mn5	2.110	1.147	2.333	151.5	152.0	172.0	−19.3	−20.6
Re1	Mn6	2.110	1.149	2.377	151.9	167.5	154.3	−6.2	−7.2
Re2	Mn1A	2.145	1.109	2.387	163.6	163.6		−13.0	−6.9
Re2	Mn2A	2.062	1.193	2.297	161.6	161.6		−18.5	−8.5
Re2	Mn3A	2.114	1.153	2.373	151.4	159.0	159.2	−13.5	−14.7
Re2	Mn4A	2.102	1.152	2.326	169.5	172.0	173.0	−4.0	−5.0
Re2	Mn5A	2.103	1.150	2.310	150.7	152.9	169.0	−18.6	−20.0
Re2	Mn6A	2.111	1.150	2.319	156.0	178.5	156.5	−2.8	−3.7

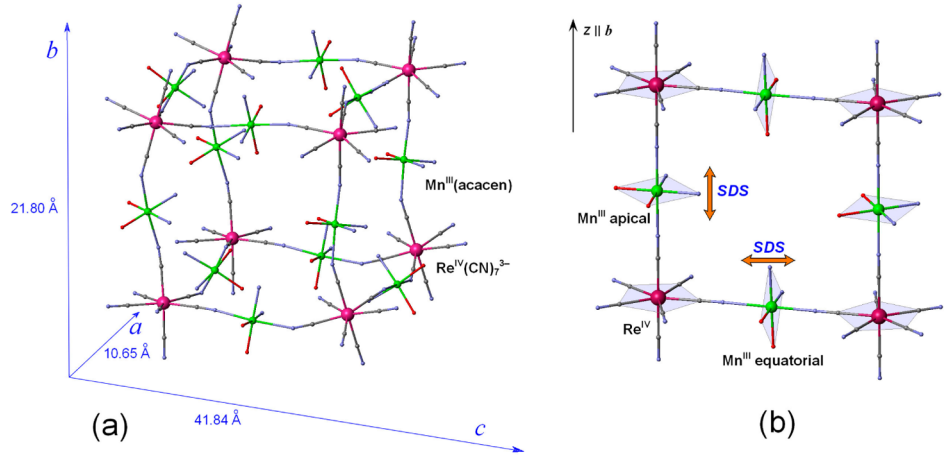

Figure 14. (a) Real low-symmetry structure of the Re−Mn bimetallic framework of **1** (C, N, and H atoms of acacen ligands are omitted for clarity); crystallographic axes *a*, *b*, *c* are shown. The polar axes of $[Re(CN)_7]^{3-}$ bipyramids are preferably oriented along the crystallographic *b* axis. (b) Idealized (symmetrized) structure of the Re−Mn framework. Apical and equatorial Mn^{III} ions are shown, and the orientation of the easy axis of the ZFS tensors of apical and equatorial Mn^{III} ions is indicated in double brown arrows. The pentagonal axis *z* of $[Re(CN)_7]^{3-}$ is parallel to the crystallographic *b* axis.

DISCUSSION

Now we can discuss in more detail the origin of anisotropic magnetic behavior of **1**. There are two internal sources of the overall magnetic anisotropy of **1**: anisotropic spin coupling of apical Re−CN−Mn linkages (Figure 13 and Table 1) and single-center ZFS anisotropy of $[Mn^{III}acacen]^+$ complexes in the bimetallic framework (Figures 1 and 14a). Note that magnetic anisotropy of individual $[Re(CN)_7]^{3-}$ low-spin complexes manifests only in the anisotropy of the ground-state *g*-tensor, $g_z = 3.66$ and $g_x = g_y = 1.59$,[24] but not in the ZFS energy, which is absent for the spin $S_{Re} = {}^1/_2$. Our calculations indicate that the anisotropy of Re−Mn spin coupling and ZFS anisotropy of Mn^{III} are comparable in magnitude. Spin coupling anisotropy is approximately estimated from the $|J_z - J_{xy}|$ difference, that ranges between 1 and 10 cm^{-1} (Table 1), while the ZFS anisotropy $|D|S^2_{Mn}$ equals typically to 10−15 cm^{-1} for square planar $[Mn^{III}SB]^+$ complexes;[9] therefore, their interplay may be the underlying cause of the anisotropic metamagnetic behavior of **1**. However, the microscopic mechanism of magnetic anisotropy in a low-symmetry 3D framework of **1** is extremely complicated due to the presence of numerous inequivalent Re−CN−Mn linkages with essentially different anisotropic exchange parameters (Table 1) and noncollinear orientation of the local magnetic axes of Mn^{III}(acacen) complexes (Figure 14). Obviously, for such a system it is very hard to provide quantitative simulation of the magnetic behavior with a conventional parametric spin Hamiltonian approach, especially below the Néel temperature T_N.

In this situation, we focus on a more qualitative data analysis. Fist we discuss possible magnetic structure of **1** below T_N. On the basis of the experimental magnetic data and results of our microscopic calculations indicating antiferromagnetic spin coupling between all Re^{IV} and Mn^{III} ions (Table 1), we can suggest a ferrimagnetic-type ordering in the 3D bimetallic framework with alternating antiparallel $S_{Re} = {}^1/_2$ and $S_{Mn} = 2$ spins (Figure 15). It is important to note that there are two distinct types of Mn^{III} ions involved, respectively, in the apical and equatorial Re−CN−Mn groups (Figure 14). Their magnetic moments may differ considerably in the amplitude and orientation due to different characters of the local anisotropic magnetic interactions.

In the 3D framework of **1**, each Mn^{III} ion is magnetically coupled with two neighboring Re^{IV} ions and undergoes single-ion ZFS splitting (Figure 14). Notably, the spin coupling

dx.doi.org/10.1021/ic501247x | Inorg. Chem. 2014, 53, 10217−10231

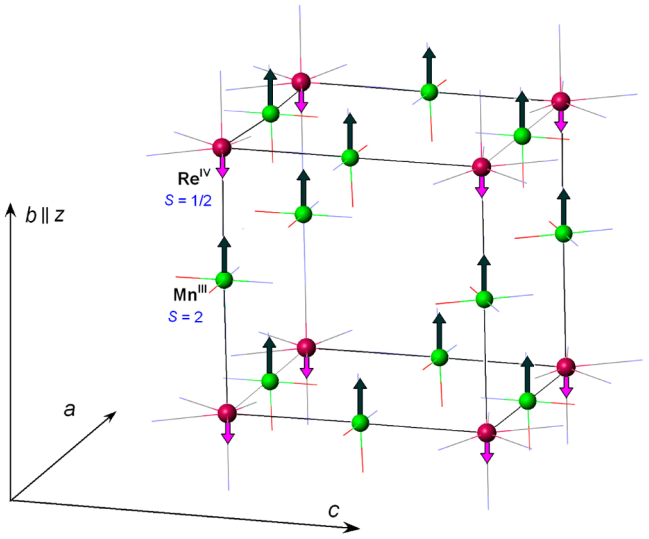

Figure 15. Supposed ferrimagnetic-type ordering in **1** below T_N in idealized structure.

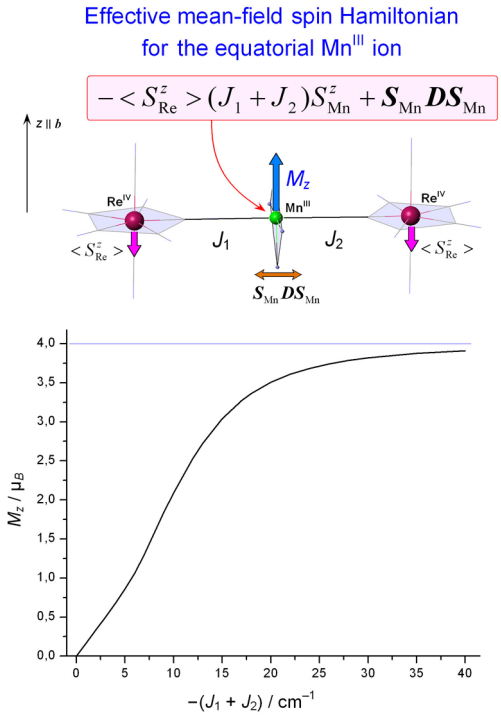

Figure 16. Effective mean-field spin Hamiltonian and calculated dependence of the M_z component for the magnetic momentum of the equatorial Mn^{III} ion on the sum $J_1 + J_2$ of the equatorial exchange parameters. The easy axis of the ZFS tensor $\mathbf{S}_{Mn}\mathbf{DS}_{Mn}$ of Mn^{III} (shown in brown double arrow) is orthogonal to the orientation of the S_{Re} spin along the polar z axis. Here M_z is the projection of the Mn^{III} magnetic moment on the polar axis z (z||b, Figure 14b).

anisotropy and ZFS anisotropy act differently for the apical and equatorial Mn^{III} ions. For the apical Mn^{III} ions, the $S_{Mn} = 2$ spin is coupled with two $S_{Re} = {}^1/_2$ spins anisotropically with an Ising-type spin Hamiltonian ($J_z > J_{xy}$, see Table 1, ions Mn1, Mn2, Mn1A, and Mn2A) that tends to align spins parallel to the local pentagonal axes of $[Re(CN)_7]^{3-}$ complexes. These axes are approximately parallel to the b axis (Figure 14a); in the idealized (symmetrized) structure of the framework, all pentagonal axes are strictly parallel to the common polar axis z (z||b, Figure 14b). The easy axis of the $\mathbf{S}_{Mn}\mathbf{DS}_{Mn}$ ZFS tensor of the apical Mn^{III} ions is also oriented along the z axis. Therefore, for the apical Mn^{III} ions both the anisotropic spin coupling and ZFS anisotropy favor for the alignment of the magnetic moment along the z axis with a maximum value of 4 μ_B. In the case of the antiferromagetic type of ordering, magnetic moment of Re^{IV} ions should be parallel to the easy b axis and antiparallel to S_{Mn} spins (Figure 15).

On the other hand, for the equatorial Mn^{III} ions the situation changes considerably since here the effective exchange molecular field of two Re^{IV} ions acts mainly on the z-component of the S_{Mn} spin, $-\langle S^z_{Re}\rangle (J_1 + J_2)S^z_{Mn}$, while the ZFS easy axis is orthogonal to the z axis (Figure 14b). As a result, the molecular field and ZFS anisotropy compete with each other resulting in a reduction of the z-component (M_z) of the Mn^{III} magnetic momentum. This effect can be simulated in terms of a simple mean-field model for a Re−Mn−Re fragment in the equatorial plane (Figure 16). The effective mean-field spin Hamiltonian for the isolated spin $S = 2$ of equatorial Mn^{III} ions can be written as

$$-\langle S^z_{Re}\rangle (J_1 + J_2)S^z_{Mn} + \mathbf{S}_{Mn}\mathbf{DS}_{Mn} \quad (5)$$

where $\langle S^z_{Re}\rangle$ is an average projection of the S_{Re} spin on the z axis and J_1 and J_2 are exchange parameters of the two Re−Mn pairs (Figure 16); here we assume isotropic spin coupling for the equatorial pairs (i.e., $J_z = J_{xy} = J_1$ or J_2) neglecting a small anisotropy component (see Figure 13 and Table 1). Assuming $\langle S^z_{Re}\rangle = -{}^1/_2$ and $D = -4.0$ cm^{-1}, $E = 0$ ZFS parameters for Mn^{III}, we evaluate the variation of the M_z component of the magnetic moment of the equatorial Mn^{III} ion as a function of $J_1 + J_2$, Figure 16.

These results elucidate why the magnetic moment of Mn^{III} ions in **1** is not perfectly oriented along the easy b axis; this is mainly due to perpendicular orientation of the easy axis of the ZFS tensor of equatorial Mn^{III} ions with respect to the b axis (Figure 14). This effect is especially pronounced at small exchange parameters in the equatorial plane: for instance, $M_z \sim 2$ at $|J_1 + J_2| = 10$ cm^{-1} (Figure 16). In this respect, Table 1 demonstrates that several equatorial Re−CN−Mn groups exhibit small exchange parameters, $|J| \sim 5$ cm^{-1} or less. Therefore, the total magnetic moment of **1** along the easy b axis may be considerably smaller than the saturation value (11 μ_B for the antiferromagnetic ordering and 13 μ_B for the ferromagnetic one), such as -1 μ_B (Re) + 4 μ_B (Mn_{apic}) + 2 × 2 μ_B (Mn_{equat}) = 7 μ_B. Qualitatively, this accounts for the fact that below T_N magnetization of **1** is not saturated in a strong magnetic field at low temperature, 8.8 μ_B at 200 mK and 8 kOe (Figure 6). It is also noteworthy that, in the real low-symmetry structure of the 3D network, the S_{Re} and S_{Mn} spins are seemingly canted due to alternating tilts of the local polar axes of $[Re(CN)_7]^{3-}$ and $[Mn(acacen)]^+$ complexes with respect to the crystallographic axes a, b, c (Figure 14a).

According to this model, maximum magnetization and magnetic susceptibility occur along the preferable orientation of the pentagonal axes of $[Re(CN)_7]^{3-}$ units, i.e., along the b axis; this is consistent with experimental finding that that b is the easy magnetic axis.

In the paramagnetic phase ($T > T_N$) magnetic properties can approximately be treated in terms of a simplified cluster model that takes into account all actual magnetic interactions in the 3D network in **1**. For this purpose, a finite $ReMn_3$ cluster with

dx.doi.org/10.1021/ic501247x | Inorg. Chem. 2014, 53, 10217−10231

one apical Re−CN−Mn group and two equatorial groups is selected in the 3D crystal structure of **1** (Figure 17); the use of this cluster reflects properly the stoichiometry of **1** and the balance between the apical and equatorial Re−CN−Mn linkages.

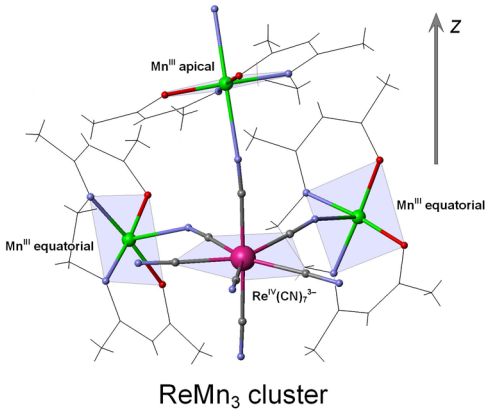

Figure 17. Structure of the $ReMn_3$ cluster used in simulation of the χT curve for the paramagnetic phase.

To interpret the experimental magnetic properties at $T > T_N$, we have diagonalized the anisotropic multispin Hamiltonian for the $ReMn_3$ cluster

$$\hat{H} = -\sum_{i=1-3} (J_{xy}^{(i)}(S_{\mathrm{Mn}(i)}^{x}S_{\mathrm{Re}}^{x} + S_{\mathrm{Mn}(i)}^{y}S_{\mathrm{Re}}^{y}) + J_{z}^{(i)}S_{\mathrm{Mn}(i)}^{z}S_{\mathrm{Re}}^{z}) + \sum_{i=1-3} \mathbf{S}_{\mathrm{Mn}(i)}(\mathbf{T}_i\mathbf{D}_i\mathbf{T}_i^{-1})\mathbf{S}_{\mathrm{Mn}(i)} + \mu_{\mathrm{B}}g_{\mathrm{Mn}}\mathbf{H}\sum_{i=1-3}\mathbf{S}_{\mathrm{Mn}(i)} + \mu_{\mathrm{B}}(g_xS_{\mathrm{Re}}^{x}H_x + g_yS_{\mathrm{Re}}^{y}H_y + g_zS_{\mathrm{Re}}^{z}H_z) \quad (6)$$

where the g_x, g_y, and g_z are components of the anisotropic g-tensor of $[Re(CN)_7]^{3-}$ (fixed at the experimental value, g_z = 3.66 and $g_x = g_y$ =1.59),[24] and $\boldsymbol{D}_i$ is the ZFS tensor for $Mn^{III}(i)$ ions (with three diagonal components E, $-E$, and D, fixed at typical Mn^{III} ZFS parameters $D = -4.0$ cm^{-1} and $E = 0$). Each $\boldsymbol{D}_i$ tensor is transformed by the $\boldsymbol{T}_i$ rotation matrix (defined by Euler rotation angles α, β, γ) specifying the orientations of these tensors in the $ReMn_3$ cluster. The spin quantization z axis is parallel to the polar pentagonal axis of the $[Re(CN)_7]^{3-}$ bipyramid (Figure 17). More details of calculations are attached in the Supporting Information.

With the largest exchange parameters obtained from microscopic calculations for the apical Re−CN−Mn group (J_z = −18, J_{xy} = −8 cm^{-1}) and equatorial groups (J_z = −19, J_{xy} = −20 cm^{-1}, Table 1), a very reasonable agreement between the experimental and simulated χT curves is observed above 30 K (using $D = -4.0$ cm^{-1}, $E = 0$, and g_{Mn} = 2.03 for Mn^{III}), Figure 18. In particular, a flat minimum in the χT curve around 75 K is well-reproduced. This minimum originates from a peculiar pattern of the spin energy spectrum of $ReMn_3$. Indeed, uniaxial anisotropic antiferromagnetic spin coupling of alternating S_{Re} = $^1/_2$ and S_{Mn} = 2 spins tends to stabilize collective spin states with large projection M_S on polar z axis of the Re site (Figure 19). In the middle energy range around 60 cm^{-1}, there is a low density of energy levels which are represented by spin states with smaller M_S spin projection; again, the upper spin states have large M_S projection (Figure 19). Therefore, at low temperature preferable thermal population of low-lying spin

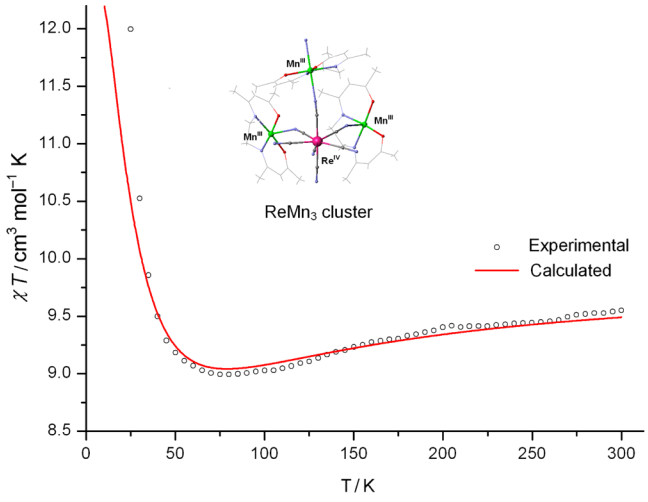

Figure 18. Comparison of the experimental χT curve (○) of 3D compound **1** and the χT curve simulated for the isolated $ReMn_3$ cluster (red line) above the Néel point T_N = 13 K. Calculations are performed with J_z = −18, J_{xy} = −8 cm^{-1} (for the apical Re−CN−Mn pair), J_z = −19, J_{xy} = −20 cm^{-1} (for the equatorial pairs), D = −4.0 cm^{-1}, E = 0 (ZFS parameters for Mn^{III} ions), g_z = 3.66, and $g_x = g_y$ = 1.59 (for $[Re(CN)_7]^{3-}$), and g_{Mn} = 2.03.

states with large M_S results in robust growth of the magnetic susceptibility below 25 K, whereas subsequent thermal population of next excited spin states results first in a flat minimum at middle temperature and then to a steady increase of χT at higher temperature (Figure 18).

Although this cluster approach cannot be applied to the analysis of magnetic ordering below T_N due to absence of extended cooperative magnetic interactions in a 3D network, it provides a qualitatively reasonable estimate of the low-temperature magnetization, namely 10.3 μ_B at 200 mK and 8 T, which is fairly comparable to the experimental value, 8.8 μ_B (Figure 6).

As was mentioned above, the magnetic properties of **1** are reminiscent of those of Mn^{II}−Mo^{III} compounds, containing $[Mo^{III}(CN)_7]^{4-}$ unit,[23a−d] a 4d electronic analogue of $[Re^{IV}(CN)_7]^{3-}$. The underlying reason is the same; i.e., strong anisotropy of exchange interactions in orbitally degenerate systems is manifesting in macroscopic magnetic phenomena such as hysterisis loops, anisotropy of magnetization, metamagnetic phase transitions, and so on. In the case of $[Mo^{III}(CN)_7]^{4-}$−Mn^{II} based compounds, strong magnetic anisotropy originated solely from Mo^{III}−Mn^{II} anisotropic spin coupling since the ZFS energy is very small for Mn^{II} ions. One more significant distinction can be seen in magnetic ordering temperature of 50 or 72 K for $K_2[Mn^{II}(H_2O)_2]_3[Mo(CN)_7]_2$[23d] that is significantly higher comparatively with 13 K for **1**. Apart from the difference between 4d and 5d orbitals and between the valence state of Mo^{III} and Re^{IV}, this is seemingly related to very long apical Mn−NC distances in Mn−NC−Re units in **1**, ∼2.337 Å vs 2.18 Å in the Mo compound. This is due to the Jahn−Teller effect in $[Mn(acacen)]^+$. As described by J. R. Long for $[L_4Mn^{II}{}_4Re(CN)_7]^{4+}$ molecular cluster,[17a] the related Mn−NC bond length is 2.169 Å, also shorter than in **1**. Long Mn^{III}−NC distances, despite the well-known anisotropy in Mn^{III} centers, are less favorable to obtain high exchange parameters. This explains why the ordering temperature in **1** is so low (13 K vs 50−72 K in Mo compounds)

dx.doi.org/10.1021/ic501247x | Inorg. Chem. 2014, 53, 10217−10231

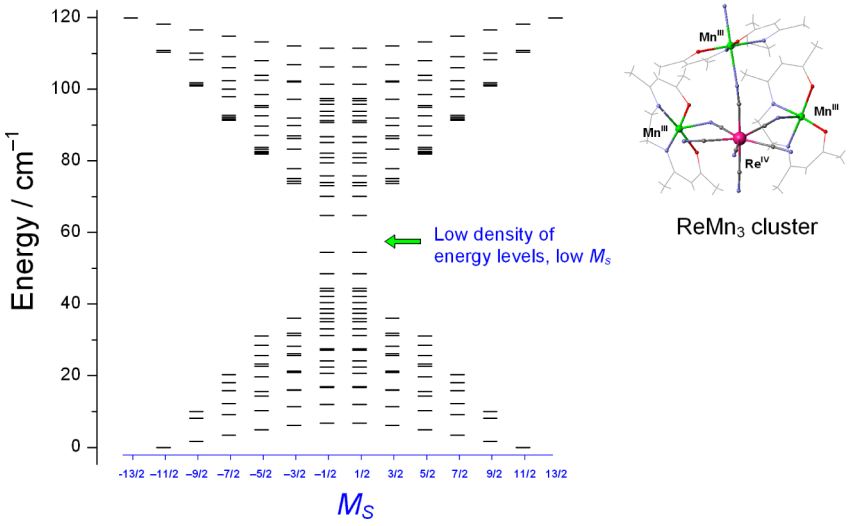

Figure 19. Calculated spin energy spectrum of the $ReMn_3$ cluster. Low density of energy levels in the middle range of the energy spectrum (represented by spin states with a small M_s spin projection) is responsible for a flat minimum in the χT curve (see Figure 18).

CONCLUSION AND PERSPECTIVES

The first heterobimetallic framework composed of homoleptic cyanometallate and a complex of Mn^{III} ion and tetradentate Schiff base ligand is prepared and characterized structurally and magnetically. The $[Mn^{III}(acacen)]_3[Re^{IV}(CN)_7]$ complex is the only example of 3D coordination polymer among the assemblies of $[Mn^{III}(Schiff\ base)]^-$ and homoleptic cyanometallates. Formation of the tridimensional framework is possible probably due to a pentagonal bipyramidal geometry of the rhenium metallo-ligand and suitable size of the constituents, as well as owing to the essential elongation of the apical bond distances in $-CN-Mn^{III}-NC$ linkages caused by the JT effect. The powder and crystal magnetic studies show the compound undergoes an antiferromagnetic ordering of a complicated character below Néel temperature of 13 K, exhibiting a metamagnetic behavior and strong magnetic anisotropy similar to those observed in related 3D $Mn^{II}-[Mo^{III}(CN)_7]^{4-}$ systems.[23] These unusual magnetic properties of $[Mn^{III}(acacen)]_3[Re^{IV}(CN)_7]$ result from a complicated interplay of Re−Mn anisotropic spin coupling and ZFS effect of Mn^{III} ions with a noncollinear orientation of the local magnetic axes in the cyano-bridged framework. A theoretical model of anisotropic spin coupling between orbitally degenerate $[Re^{IV}(CN)_7]^{3-}$ complexes and Mn^{III} ions is developed, and specific microscopic mechanisms of highly anisotropic spin coupling in $Re^{IV}-CN-Mn^{III}$ linkages in compound **1** are analyzed in detail. These theoretical results are used in the interpretation of anisotropic magnetic properties of **1** and its metamagnetic behavior below the Néel temperature. Further development of our synthetic approach is focused on obtaining discrete clusters (0D) and chain polymers (1D) involving $[Re^{IV}(CN)_7]^{3-}$ and $[Mn^{III}SB]^+$ complexes; this work is underway.

ASSOCIATED CONTENT

Supporting Information

Additional details, figures, and tables. Crystallographic data in CIF format. This material is available free of charge via the Internet at http://pubs.acs.org. These data can also be obtained free of charge from the Cambridge Crystallographic Data Centre via www.ccdc.cam.ac.uk/data_request/cif, with deposition number CCDC 874377.

AUTHOR INFORMATION

Corresponding Authors

*E-mail: Carley.Paulsen@neel.cnrs.fr.
*E-mail: mirsa@list.ru.
*E-mail: vosk@niic.nsc.ru. Fax: 7 3833309489. Phone: 7 3833309490

Notes

The authors declare no competing financial interest.

ACKNOWLEDGMENTS

This research was supported in part by RFBR (Grant 08-03-00459-a) and REA (FP7-PEOPLE-2011-IIF Proposal 301689). K.E.V. dedicates this article to the memory of Paul Rey, a true friend and teacher.

REFERENCES

(1) (a) Letard, J. F. *J. Mater. Chem.* **2006**, *16*, 2550−2559. (b) Guetlich, P.; Goodwin, H. A. *Top. Curr. Chem.* **2004**, *233*, 1−47. (c) Murray, K. S.; Kepert, C. J. *Top. Curr. Chem.* **2004**, *233*, 195−228. (d) Letard, J. F.; Guionneau, P.; Goux-Capes, L. *Towards Spin Crossover Applications*; Springer-Verlag: Berlin, 2004; Vol. *235*, pp 221−249. (e) Herchel, R.; Boca, R.; Gembicky, M.; Kozisek, J.; Renz, F. *Inorg. Chem.* **2004**, *43*, 4103−4105. (f) Real, J. A.; Gaspar, A. B.; Munoz, M. C.; Gutlich, P.; Ksenofontov, V.; Spiering, H. *Top. Curr. Chem.* **2004**, *233*, 167−193.

(2) (a) Mathoniere, C.; Podgajny, R.; Guionneau, P.; Labrugere, C.; Sieklucka, B. *Chem. Mater.* **2005**, *17*, 442−449. (b) Li, D.; Clerac, R.; Roubeau, O.; Harte, E.; Mathoniere, C.; Le Bris, R.; Holmes, S. M. *J. Am. Chem. Soc.* **2008**, *130*, 252−258. (c) Liu, T.; Zhang, Y.-J.; Kanegawa, S.; Sato, O. *J. Am. Chem. Soc.* **2010**, *132*, 8250−8251.

(3) (a) Sessoli, R.; Gatteschi, D.; Caneschi, A.; Novak, M. A. *Nature* **1993**, *365*, 141−143. (b) Tsai, H. L.; Eppley, H. J.; Devries, N.; Folting, K.; Christou, G.; Hendrickson, D. N. *Chem. Commun.* **1994**, 1745−1746. (c) Murugesu, M.; Takahashi, S.; Wilson, A.; Abboud, K. A.; Wernsdorfer, W.; Hill, S.; Christou, G. *Inorg. Chem.* **2008**, *47*, 9459−9470. (d) Schelter, E. J.; Karadas, F.; Avendano, C.; Prosvirin, A. V.; Wernsdorfer, W.; Dunbar, K. R. *J. Am. Chem. Soc.* **2007**, *129*, 8139−8149. (e) Li, D.; Parkin, S.; Clerac, R.; Holmes, S. M. *Inorg. Chem.* **2006**, *45*, 7569−7571. (f) Beedle, C. C.; Stephenson, C. J.;

Heroux, K. J.; Wernsdorfer, W.; Hendrickson, D. N. *Inorg. Chem.* **2008**, *47*, 10798−10800.
(4) (a) Leuenberger, M. N.; Loss, D. *Nature* **2001**, *410*, 789−793. (b) Wernsdorfer, W.; Allaga-Alcalde, N.; Hendrickson, D. N.; Christou, G. *Nature* **2002**, *416*, 406−409. (c) Hill, S.; Edwards, R. S.; Aliaga-Alcalde, N.; Christou, G. *Science* **2003**, *302*, 1015−1018. (d) Lehmann, J.; Gaita-Arino, A.; Coronado, E.; Loss, D. *Nat. Nanotechnol.* **2007**, *2*, 312−317. (e) Bogani, L.; Wernsdorfer, W. *Inorg. Chim. Acta* **2008**, *361*, 3807−3819. (f) Winpenny, R. E. P. *Angew. Chem., Int. Ed.* **2008**, *47*, 7992−7994. (g) Bogani, L.; Wernsdorfer, W. *Inorg. Chim. Acta* **2008**, *361*, 3807−3819. (h) Bogani, L.; Wernsdorfer, W. *Nat. Mater.* **2008**, *7*, 179−186. (i) Winpenny, R. E. P. *Angew. Chem., Int. Ed.* **2008**, *47*, 7992−7994. (j) Timco, G. A.; Carretta, S.; Troiani, F.; Tuna, F.; Pritchard, R. G.; McInnes, E. J. L.; Ghirri, A.; Candini, A.; Santini, P.; Amoretti, G.; Affronte, M.; Winpenny, R. E. P. *Nat. Nanotechnol.* **2009**, *4*, 173−178. (k) Troiani, F.; Affronte, M. *Chem. Soc. Rev.* **2011**, *40*, 3119−3129. (l) Sanvito, S. *Chem. Soc. Rev.* **2011**, *40*, 3336−3355. (m) Camarero, J.; Coronado, E. *J. Mater. Chem.* **2009**, *19*, 1678−16. (n) Clemente-Juan, J. M.; Coronado, E.; Gaita-Ariño, A. *Chem. Soc. Rev.* **2012**, *41*, 7464−7478. Aromí, G.; Aguilà, D.; Gamez, P.; Luis, F.; Roubeau, O. *Chem. Soc. Rev.* **2012**, *41*, 537−546.
(5) (a) Pan, D.; Caruthers, S. D.; Senpan, A.; Schmieder, A. H.; Wickline, S. A.; Lanza, G. M. *Nanomed. Nanobiotechnol.* **2011**, *3*, 162−173. (b) Rosenholm, J. M.; Sahlgren, C.; Linden, M. *Nanoscale* **2010**, *2*, 1870−1883. (c) Arias, J. L. *Expert Opin. Drug Delivery* **2011**, *8*, 1589−1608. (d) Choi, H. S.; Frangioni, J. V. *Mol. Imaging* **2010**, *9*, 291−310. (e) Bae, K. H.; Chung, H. J.; Park, T. G. *Mol. Cells* **2011**, *31*, 295−302.
(6) Dunbar, K. R. *Inorg. Chem.* **2012**, *51*, 12055−12058.
(7) (a) Caneschi, A.; Gatteschi, D.; Lalioti, N.; Sangregorio, C.; Sessoli, R.; Venturi, G.; Vindigni, A.; Rettori, A.; Pini, M. G.; Novak, M. A. *Angew. Chem., Int. Ed.* **2001**, *40*, 1760−1763. (b) Clérac, R.; Miyasaka, H.; Yamashita, M.; Coulon, C. *J. Am. Chem. Soc.* **2002**, *124*, 12837−12844. (c) Coulon, C.; Miyasaka, H.; Clérac, R. *Struct. Bonding (Berlin)* **2006**, *122*, 163−206. (d) Bogani, L.; Vindigni, A.; Sessoli, R.; Gatteschi, D. *J. Mater. Chem.* **2008**, *18*, 4750−4758. (d) Pełka, R.; Bałanda, M.; Przychodzeń, P.; Tomala, K.; Sieklucka, B.; Wasiutyński, T. *Phys. Status Solidi C* **2006**, *3*, 216−219. (e) Sun, H.-L.; Wang, Z.-M.; Gao, S. *Coord. Chem. Rev.* **2010**, *254*, 1081−1100. (f) Clérac, R.; Miyasaka, H.; Yamashita, M.; Coulon, C. *J. Am. Chem. Soc.* **2002**, *124*, 12837−12844. (g) Feng, X.; Harris, T. D.; Hill, S.; Long, J. R. *Chem. Sci.* **2011**, *2*, 1688−1694. (k) Harris, T. D.; Bennett, M. V.; Clérac, R.; Long, J. R. *J. Am. Chem. Soc.* **2010**, *132*, 3980−3988. (h) Miyasaka, H.; Madanbashi, T.; Sugimoto, K.; Nakazawa, Y.; Wernsdorfer, W.; Sugiura, K.; Yamashita, M.; Coulon, C.; Clerac, R. *Chem.—Eur. J.* **2006**, *12*, 7028−7040. (i) Ferbinteanu, M.; Miyasaka, H.; Wernsdorfer, W.; Nakata, K.; Sugiura, K.; Yamashita, M.; Coulon, C.; Clerac, R. *J. Am. Chem. Soc.* **2005**, *127*, 3090−3099.
(8) (a) Mironov, V. S. *Dokl. Phys. Chem.* **2006**, *408*, 130−136. (b) Waldmann, O. *Inorg. Chem.* **2007**, *46*, 10035−10037. (b) Mironov, V. S.; Chibotaru, L. F.; Ceulemans, A. *J. Am. Chem. Soc.* **2003**, *125*, 9750−9760. (c) Mironov, V. S. *Dokl. Phys. Chem.* **2007**, *415*, 199−204. (d) Ruiz, E.; Cirera, J.; Cano, J.; Alvarez, S.; Loose, C.; Kortus, J. *Chem. Commun.* **2008**, 52−54.
(9) (a) Boča, R. *Coord. Chem. Rev.* **2004**, *248*, 757−815. (b) Boča, R. *Struct. Bonding (Berlin)* **2006**, *117*, 1−264.
(10) (a) Benelli, C.; Gatteschi, D. *Chem. Rev.* **2002**, *102*, 2369−2387. (b) Sessoli, R.; Powell, A. K. *Coord. Chem. Rev.* **2009**, *253*, 2328−2341. (c) Sorace, L.; Benelli, C.; Gatteschi, D. *Chem. Soc. Rev.* **2011**, *40*, 3092−3104. (d) Woodruff, D. N.; Winpenny, R. E. P.; Layfield, R. A. *Chem. Rev.* **2013**, *113*, 5110−5148.
(11) (a) Blagg, R. J.; Muryn, C. A.; McInnes, E. J. L.; Tuna, F.; Winpenny, R. E. P. *Angew. Chem., Int. Ed.* **2011**, *50*, 6530−6533. (b) Blagg, R. J.; Tuna, F.; McInnes, E. J. L.; Winpenny, R. E. P. *Chem. Commun.* **2011**, *47*, 10587−10589.
(12) Habib, F.; Murugesu, M. *Chem. Soc. Rev.* **2013**, *42*, 3278−3288.
(13) (a) Rinehart, J. D.; Fang, M.; Evans, W. J.; Long, J. R. *J. Am. Chem. Soc.* **2011**, *133*, 14236−14236. (b) Rinehart, J. D.; Fang, M.; Evans, W. J.; Long, J. R. *Nat. Chem.* **2011**, *3*, 538−542.
(14) Wang, X.-Y.; Avendano, C.; Dunbar, K. R. *Chem. Soc. Rev.* **2011**, *40*, 3213−3238.
(15) Dreiser, J.; Pedersen, K. S.; Schnegg, A.; Holldack, K.; Nehrkorn, J.; Sigrist, M.; Tregenna-Piggott, P.; Mutka, H.; Weihe, H.; Mironov, V. S.; Bendix, J.; Waldmann, O. *Chem.—Eur. J.* **2013**, *19*, 3693−3701.
(16) Qian, K.; Huang, X.-C.; Zhou, C.; You, X.-Z.; Wang, X.-Y.; Dunbar, K. R. *J. Am. Chem. Soc.* **2013**, *135*, 13302−13305.
(17) (a) Freedman, D. E.; Jenkins, D. M.; Iavarone, A. T.; Long, J. R. *J. Am. Chem. Soc.* **2008**, *130*, 2884−2885. (b) Zadrozny, J. M.; Freedman, D. E.; Jenkins, D. M.; Harris, T. D.; Iavarone, A. T.; Mathoniere, C.; Clérac, R.; Long, J. R. *Inorg. Chem.* **2010**, *49*, 8886−8896. (c) Harris, T.; Bennett, M.; Clérac, R.; Long, J. R. *J. Am. Chem. Soc.* **2010**, *132*, 3980−3988. (d) Harris, T. D.; Soo, H. S.; Chang, C.; Long, J. R. *Inorg. Chim. Acta* **2011**, *369*, 91−96. (e) Feng, X.; Harris, T. D.; Long, J. R. *Chem. Sci.* **2011**, *2*, 1688−1694. (f) Feng, X.; Liu, J.; Harris, T. D.; Hill, S.; Long, J. R. *J. Am. Chem. Soc.* **2012**, *134*, 7521−7529. (g) Bhowmick, I.; Harris, D. T.; Dechambenoit, P.; Hillard, E. A.; Pichon, C.; Jeon, I.-R.; Clérac, R. *Sci. China: Chem.* **2012**, *55*, 1004−1011.
(18) (a) Pedersen, K. S.; Bendix, J.; Clérac, R. *Chem. Commun.* **2014**, *50*, 4396−4415 and references therein. (b) Zhang, W.-X.; Breedlove, B.; Ishikawa, R.; Yamashita, M. *RSC Adv.* **2013**, *3*, 3772−3798 and references therein.
(19) (a) Yeung, W. F.; Lau, P. H.; Lau, T. C.; Wei, H. Y.; Sun, H. L.; Gao, S.; Chen, Z. D.; Wong, W. T. *Inorg. Chem.* **2005**, *44*, 6579−6590. (b) Pedersen, K. S.; Dreiser, J.; Nehrkorn, J.; Gysler, M.; Schau-Magnussen, M.; Schnegg, A.; Holldack, K.; Bittl, R.; Piligkos, S.; Weihe, H.; Tregenna-Piggott, P.; Waldmann, O.; Bendix, J. *Chem. Commun.* **2011**, *47*, 6918−6920. (c) Ru, J.; Gao, F.; Wu, T.; Yao, M.-X.; Li, Y.; Zuo, J.-L. *Dalton Trans.* **2014**, *43*, 933−936.
(20) (a) Hilfiger, M. G.; Shatruk, M.; Prosvirin, A.; Dunbar, K. R. *Chem. Commun.* **2008**, 5752−5754. (b) Hilfiger, M. G.; Chen, M.; Brinzari, T. V.; Nocera, T. M.; Shatruk, M.; Petasis, D. T.; Musfeldt, J. L.; Achim, C.; Dunbar, K. R. *Angew. Chem., Int. Ed.* **2010**, *49*, 1410−1413. (c) Pedersen, K. S.; Schau-Magnussen, M.; Bendix, J.; Weihe, H.; Palii, A. V.; Klokishner, S. I.; Ostrovsky, S.; Reu, O. S.; Mutka, H.; Tregenna-Piggott, P. L. W. *Chem.—Eur. J.* **2010**, *16*, 13458−13464. (d) Hoeke, V.; Stammler, A.; Bögge, H.; Schnack, J.; Glaser, T. *Inorg. Chem.* **2014**, *53*, 257−268.
(21) (a) Miyasaka, H.; Matsumoto, N.; Okawa, H.; Re, N.; Gallo, E.; Floriani, C. *J. Am. Chem. Soc.* **1996**, *118*, 981−994. (b) Choi, H. J.; Sokol, J. J.; Long, J. R. *Inorg. Chem.* **2004**, *43*, 1606−1608. (c) Ferbinteanu, M.; Miyasaka, H.; Wernsdorfer, W.; Nakata, K.; Sugiura, K.-I.; Yamashita, M. M.; Coulon, C.; Clerac, R. *J. Am. Chem. Soc.* **2005**, *127*, 3090−3099. (d) Tregenna-Piggott, P. L. W.; Sheptyakov, D.; Keller, L.; Klokishner, S. I.; Ostrovsky, S. M.; Palii, A. V.; Reu, O. S.; Bendix, J.; Brock- Nannestad, T.; Pedersen, K.; Weihe, H.; Mutka, H. *Inorg. Chem.* **2009**, *48*, 128−137. (e) Dreiser, J.; Schnegg, A.; Holldack, K.; Pedersen, K. S.; Schau-Magnussen, M.; Nehrkorn, J.; Tregenna-Piggott, P.; Mutka, H.; Weihe, H.; Bendix, J.; Waldmann, O. *Chem.—Eur. J.* **2011**, *17*, 7492−7498. (f) Miyasaka, H.; Madanbashi, T.; Saitoh, A.; Motokawa, N.; Ishikawa, R.; Yamashita, M.; Bahr, S.; Wernsdorfer, W.; Clérac, R. *Chem.—Eur. J.* **2012**, *18*, 3942−3954. (g) Peresypkina, E. V.; Majcher, A. M.; Rams, M.; Vostrikova, K. E. *Chem. Commun.* **2014**, *50*, 7150−7153.
(22) Miyasaka, H.; Clerac, R.; Wernsdorfer, W.; Lecren, L.; Bonhomme, C.; Sugiura, K.-I.; Yamashita, M. *Angew. Chem., Int. Ed.* **2004**, *43*, 2801−2805.
(23) (a) Larionova, J.; Clérac, R.; Sanchiz, J.; Kahn, O.; Golhen, S.; Ouahab, L. *J. Am. Chem. Soc.* **1998**, *120*, 13088−13095. (b) Kahn, O.; Larionova, J.; Ouahab, L. *Chem. Commun.* **1999**, 945−952. (c) Kahn, O.; Larionova, J.; Ouahab, L. *Chem. Commun.* **1999**, 945−952. (d) Larionova, J.; Kahn, O.; Gohlen, S.; Ouahab, L.; Clérac, R. *J. Am. Chem. Soc.* **1999**, *121*, 3349−3356. (e) Wang, Q.-L.; Southerland, H.; Li, J.-R.; Prosvirin, A. V.; Zhao, H.; Dunbar, K. R. *Angew. Chem., Int. Ed.* **2012**, *51*, 9321−9324.
(24) Bennett, M. V.; Long, J. R. *J. Am. Chem. Soc.* **2003**, *125*, 2394−2395.

(25) Peresypkina, E. V.; Vostrikova, K. E. *Dalton Trans.* **2012**, *41*, 4100−4106.
(26) Boucher, L. J.; Day, V. W. *Inorg. Chem.* **1977**, *16*, 1360−1367.
(27) Bain, G. A.; Berry, J. F. *J. Chem. Educ.* **2008**, *85*, 532−533.
(28) (a) Sheldrick, G. M. *Acta Crystallogr.* **2008**, *A64*, 112−122. (b) *Bruker Advanced X-ray Solutions*; Bruker AXS Inc.: Madison, WI, 2004.
(29) Mironov, V. S.; Chibotaru, L. F.; Ceuleman, A *Phys. Rev. B* **2003**, *67*, 014424−014428.